

Random coupling models for intramolecular dynamics. I. Mathematical approach^{a)}

Benny Carmeli^{b)} and Abraham Nitzan^{b)}

Department of Chemistry, Tel-Aviv University, Tel Aviv, Israel
(Received 1 March 1979; accepted 31 1979)

Intramolecular dynamics in large molecules is modeled as a problem involving random coupling between manifolds of molecular levels. The random coupling model (RCM) is based on the rapid variations observed in coupling matrix elements involving highly excited bound molecular states, and on the high density of such states encountered in large molecules. The finite time and energy scales involved in real experimental situations lead to the observation that the time evolution and spectral properties characterizing the system do not depend on the detailed arrangement of states and their coupling elements but rather on low order moments of the distribution characterizing these coupling elements. This provides the basis for an approach based on ensemble averages. The coupling V is taken as a superposition $V = u + v$ of a smoothly varying component $u = \langle V \rangle$ and a randomly varying (in state space) component $v = V - \langle V \rangle$. We introduce a diagrammatic expansion and averaging method to evaluate the diadic Green's function for problems involving absorption line shapes, and a similar approach for the evaluation of the tetradic Green's function used in calculations of time evolution. With these methods, we study the time evolution in systems involving discrete states and quasicontinuous manifolds. The solution is relevant for multiphoton excitation of large molecules, and for intramolecular electronic and vibrational transitions. We also study the effect of random coupling in absorption line shapes involving interference between resonances or interference between a resonance and a background absorptions. The mechanism for coherence erosion resulting from the random behavior of the coupling is elucidated.

I. INTRODUCTION

Intramolecular dynamics, namely, the pathways and the corresponding rates associated with molecular energy redistribution, rearrangement, and dissociation under collisionless conditions, has long been an outstanding experimental and theoretical problem.¹ Increasing attention has been recently given to the application of random coupling models (RCM's) in the theories of such intramolecular processes.²⁻¹² These processes may be described in terms of coupling elements between zero order molecular states which are wildly varying as functions of state energy or state index. This rapid variation results from the fact that these elements are essentially overlap integrals between molecular bound states which are, for highly excited states, strongly oscillatory. In spectral regions of high density of states such coupling may be modeled by some random distribution.

RCM's have so far been considered with respect to various intramolecular dynamics problems. Gelbart, Freed, and Rice² and Kay⁵ have applied such models for the problem of intramolecular vibrational relaxation (IVR) in large molecules. Heller and Rice⁶ have applied a separable random coupling model to discuss molecular predissociation. An RCM has been used by Delory and Tric³ and by Gelbart, Heller, and Elert⁴ to discuss intramolecular electronic relaxation (IER) in large molecules. Druger⁸ has applied RCM to study the erasure of interference effects associated with the interaction of discrete levels with quasicontinuous molecular manifolds. Recently such models have been utilized by Schek

and Jortner¹² and by Carmeli and Nitzan^{10,11} to rationalize the loss of coherence in collisionless IR multiphoton excitation and dissociation of large molecules, and by Nitzan and Jortner¹³ to discuss the IR induced inverse electronic relaxation in large molecules. It should be mentioned that RCM's have a long history in the theory of nuclear spectra¹⁴ and in theories of random solids.¹⁵

While RCM's for absorption line shapes are relatively easy to solve (an elegant solution has been provided by Druger⁸) the calculation of scattering line shapes or the time evolution associated with these RCM's constitutes substantially more difficult problems. The situation is similar to that encountered in the theories of nuclear spectra¹⁴ and of random solids.¹⁵ The density of levels (i.e., the distribution of eigenvalues of the relevant random matrices) has been obtained within certain approximations (for some models exactly) while the corresponding dynamical problem is still essentially unsolved. Mathematically, the difference lies in the fact that the spectral problem requires the evaluation of the averaged diadic Green's function for the system, while the dynamical problem is associated with the averaged tetradic Green's function (or, equivalently, the average of the absolute square of the diadic Green's function).

We have recently described an approach¹¹ which makes it possible to obtain explicit solutions for the time evolution associated with intercontinuum random coupling models. Our approach is based on a diagrammatic expansion and averaging of the tetradic Green's function. Having this, the method can be also applied to obtain cross sections for light scattering of systems characterized by random coupling. The present article provides the mathematical details of this approach and describes some applications. In subsequent publications we shall apply this method to multiphoton excitation dynamics in large molecules¹⁶ and to the problem of light scattering from such molecules.¹⁷

^{a)}Supported in part by the United States-Israel Binational Science Foundation, Jerusalem, Israel and by the Commission for Basic Research of the Israel Academy of Science.

^{b)}Present address: Bell Laboratories, Murray Hill, N. J. 07974.

Attempts to obtain the time evolution associated with RCM's have been recently made by other authors. Heller and Rice⁶ have obtained the time evolution of a separable (see Sec. II) RCM under assumptions which strongly restrict the validity of their results.¹⁸ Schek and Jortner¹² have described an approach based on the derivation of the master equation from the Schrödinger equation.^{5,19} They had to resort however to some assumptions of unclear basis in the course of their derivation. Kay⁵ has applied an RCM for the problem of intramolecular vibrational relaxation. Some of his qualitative ideas are incorporated into the model introduced in Sec. II. Our mathematical approach is very different from his and allows for a more direct and explicit evaluation of observable quantities in the presence of both random and smoothly varying components in the intramolecular coupling.

To end these introductory remarks, it should be pointed out that the intercontinuum coupling models have a wide range of applications in molecular dynamics problems. Such models have been applied in the theories of photodissociation and predissociation of polyatomic molecules,^{20,21} vibrational predissociation of van der Waals complexes,²² the relaxation of excited atoms by collisions with diatomic molecules,²³ multiphoton IR excitation and dissociation of large molecules,^{10,11,17,24,25} and multiphoton IR induced inverse electronic relaxation.¹³ For some of these problems (e.g., dissociation of a triatomic molecule,²¹ predissociation of small van der Waals complexes,²² and relaxation of excited atoms by diatomics²³) the constant intercontinuum coupling model has been applied as a reasonable approximation. For the others the corresponding RCM is more appropriate.

The following section describes the model and assumptions invoked in our solution. Section III introduces the diagrammatic technique and demonstrates its use for the familiar model consisting of a discrete level interacting with a continuum or a dense manifold ("quasi-continuum") of levels. In Sec. IV we apply this technique to the problem of time evolution in an intercontinuum coupling model, which is suitable for problems like intramolecular vibrational relaxation and molecular multiphoton excitation. In Sec. V we describe the application of this approach to problems involving interference effects in absorption line shapes. We conclude by discussing the significance of the solution obtained. More detailed applications will be presented in subsequent papers.^{16,17}

II. MODEL AND ASSUMPTIONS

The most general model that is treated by our approach is displayed schematically in Fig. 1. It consists of a few discrete levels $|0\rangle, |1\rangle, \dots, |I-1\rangle$ and a few dense manifolds $\{|I, \alpha\rangle\}, \{|I+1, \alpha\rangle\}, \dots, \{|M, \alpha\rangle\}$ where α denotes the level index within the particular manifold. The discrete levels and the levels of the different manifolds are coupled to each other, but levels belonging to the same manifold are not. Depending on the physical problem we may be interested in absorption and scattering cross-sections associated with some of the discrete

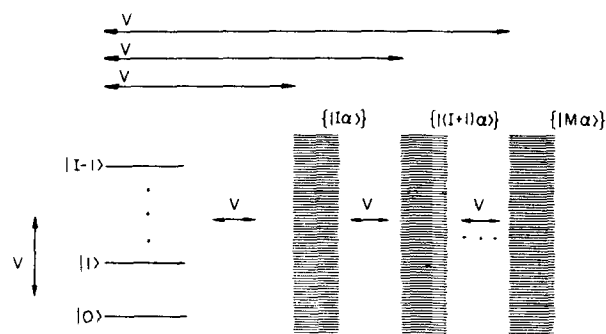


FIG. 1. A general system of coupled molecular discrete levels and quasicontinuous manifolds. This system is a generalization of all models discussed in this paper. V denotes an intramolecular or an externally induced coupling.

levels as initial and final states, while the rest of the discrete levels and all the continuous manifolds provide the set of intermediate molecular states; or alternatively in the time evolution of the populations $P_0 \dots P_{I-1}, P_I \equiv \sum_{\alpha} P_{I\alpha} \dots P_M \equiv \sum_{\alpha} P_{M\alpha}$ and of the nondiagonal matrix elements of the density operator associated with the discrete set $0 \dots I-1$. It is essential to our approach that we do not seek any information about individual levels $|J\alpha\rangle$ of the dense manifolds.

Consider now the coupling elements $V_{J\alpha, J'\alpha'}(J, J' \geq I)$ or $V_{J, J'\alpha'}(J < I, J' \geq I)$. Throughout this paper we assume for the sake of simplicity that all these coupling terms are real. We distinguish between different kinds of coupling models:

(a). In the constant coupling model (CCM) $V_{J\alpha, J'\alpha'}$ and $V_{J, J'\alpha'}$ are taken to be independent of α and α' .

$$V_{J\alpha, J'\alpha'} = u_{JJ'}; \quad V_{J, J'\alpha'} = u_{JJ'}. \quad (\text{II. 1})$$

(b). In the random coupling model (RCM) $V_{J\alpha, J'\alpha'}$ and $V_{J, J'\alpha'}$ are assumed to be random functions of α and α' such that

$$\langle V_{J\alpha, J'\alpha'} \rangle = u_{JJ'}; \quad \langle V_{J, J'\alpha'} \rangle = u_{JJ'}, \quad (\text{II. 2})$$

where the averages are defined from

$$\langle V_{J\alpha, J'\alpha'} \rangle = \frac{1}{NN'} \sum_{\alpha} \sum_{\alpha'} V_{J\alpha, J'\alpha'} \quad (\text{II. 3})$$

$$\langle V_{J, J'\alpha'} \rangle = \frac{1}{N'} \sum_{\alpha'} V_{J, J'\alpha'}, \quad (\text{II. 4})$$

and where N and N' being the number of levels contributing to the sums over α and α' , respectively. The case where $u_{JJ'} = 0$ is referred to as the completely random or the symmetric random model. More generally we may have an asymmetric distribution where $u_{JJ'} \neq 0$. We write

$$\begin{aligned} V_{J\alpha, J'\alpha'} &= u_{JJ'} + v_{J\alpha, J'\alpha'} \\ V_{J, J'\alpha'} &= u_{JJ'} + v_{J, J'\alpha'} \end{aligned} \quad (\text{II. 5})$$

with

$$\langle v_{J\alpha, J'\alpha'} \rangle = \langle v_{J, J'\alpha'} \rangle = 0. \quad (\text{II. 6})$$

(c). The separable random coupling model is defined as in the RCM, only intercontinuum coupling elements are assumed to be separable into products of terms

$$V_{J\alpha, J'\alpha'} = V_{J\alpha} \cdot V_{J'\alpha'}, \quad (\text{II. 7})$$

where $V_{J\alpha}$ and $V_{J'\alpha'}$ are independent random functions of the α and α' indices with $\langle V_{J\alpha} \rangle = 0$ in the symmetric (totally random) case and $\langle V_{J\alpha} \rangle \neq 0$ in the asymmetric case.

To understand the scope and limitations of these models, it is important to introduce the coarse grained nature of the averages (II. 3). We assume that:

(1). The manifolds are dense, that is the average level spacing ρ_J^{-1} in the manifold $J(J \geq I)$ is much smaller relative to the inverse experimental timescale τ^{-1}

$$\hbar\rho_J \gg \tau \quad (J \geq I). \quad (\text{II. 8})$$

(2). The coupling elements $V_{J\alpha, J'\alpha'}$ and $V_{J, J'\alpha'}$ vary on two vastly different energy scales. There are rapid, essentially random, variations over energy distance of order ρ^{-1} (i.e., the level spacing). These variations are uncorrelated: the coupling elements involving the level $|J\alpha\rangle$ are independent of those involving the level $|J\alpha'\rangle$ ($\alpha \neq \alpha'$) even for nearest neighbors α and α' . In addition there may be a slow systematic change in the coupling over a much larger energy scale ΔE .

It is then possible to divide any manifold J ($J \geq I$) into energy intervals ϵ satisfying

$$\begin{aligned} \hbar\rho_J &\gg \hbar/\epsilon \gg \tau \quad (J \geq I) \\ \epsilon &\ll \Delta E, \end{aligned} \quad (\text{II. 9})$$

and to define the averages (II. 3) as coarse grained averages over such intervals. In doing so we separate between the rapid "random" variation and between the slow systematic change of the coupling with the level indices. This systematic change is reflected in the residual weak α dependence of averages like $\langle V_{J\alpha, J'\alpha'} \rangle$ ($J, J' \geq I$) or $\langle V_{J, J'\alpha'} \rangle$ ($J < I, J' \geq I$); also of higher moments like $\langle V_{J\alpha, J'\alpha'}^2 \rangle$ or $\langle V_{J, J'\alpha'}^2 \rangle$. The weak systematic change was neglected in Eqs. (II. 1, 2).

Having defined these coarse grained averages we further assume

(3). A systematic variation of the coupling occurs only over energy ranges much larger than the inverse experimental time scale. The inequalities (II. 9) thus take the form

$$\hbar\rho_J \gg \hbar/\epsilon \gg \tau \gg \hbar/\Delta E \quad (J \geq I). \quad (\text{II. 10})$$

Equation (II. 10) relates the relative magnitudes of three energy scales: The average level spacing ρ_J^{-1} which by assumption (2) measures also the correlation length (in energy space) for the random variation of the coupling, the inverse experimental time scale τ^{-1} and the energy range ΔE for the systematic variation of the coupling. The separation between these scales enables us to introduce the coarse grained average defined over intervals of energy lengths ϵ . A pictorial representation of this situation is displayed in Fig. 2. Similar assumptions characterize the RCM which was studied by Kay.⁵

The calculation described in the following sections is facilitated by introducing two further ideas by way of the following assumptions:

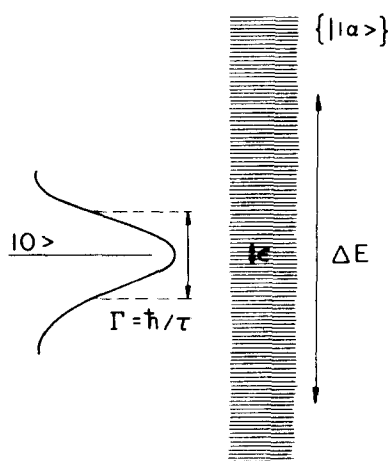


FIG. 2. A demonstration of orders of magnitudes for different molecular and experimental parameters. The quantities which appear here are defined in the text.

(4). The physical observables of the system depend only on the distribution of the random coupling elements and not on the detailed dependence of these elements on the level indices α . The rationale behind this assumption lies in the orders of magnitude expressed by (II. 10) and Fig. 2. The essential point is the existence of an interval which is much smaller than the uncertainty width \hbar/τ of the individual levels, but large enough to encompass enough levels so that the distribution of coupling elements is essentially sampled within this interval. Under these conditions the detailed dependence of the elements $V_{J\alpha, J'\alpha'}$ (or $V_{J, J'\alpha'}$) on the level indices α and α' within such intervals (as opposed to the slow systematic variation) should not influence the observed quantities.

(5). The behavior of the system is characterized mostly by the lower moments (average and variance) of the random coupling distribution and is not strongly affected by finer details (higher moments) of this distribution. The plausibility of this assumption results again from inequalities (II. 10). These inequalities suggest that we may group levels together over intervals ϵ' which satisfy $\epsilon \gg \epsilon' \gg \rho^{-1}$ and consider the effective coupling between such groups. The central limit theorem of probability theory then implies that this effective coupling will be a Gaussian random variable which is characterized by its two lowest moments.

Assumption (4) enables us to introduce the idea of *ensemble averaging*: Since the physically interesting dynamics is determined by the distribution of coupling elements and not by their detailed values, we may consider an ensemble of molecules, all characterized by this same distribution and take averages of observable quantity over this ensemble. By assumption (2) we then have

$$\langle v_{J\alpha, J'\alpha'} \rangle = \langle v_{J'\alpha', J\alpha} \rangle = 0 \quad (\text{II. 11})$$

$$\begin{aligned} \langle v_{J\alpha, J'\alpha'} \cdot v_{K\beta, K'\beta'} \rangle &= \langle v_{J\alpha, J'\alpha'}^2 \rangle (\delta_{JK} \delta_{J'K'} \delta_{\alpha\beta} \delta_{\alpha'\beta'}) \\ &\quad + \delta_{J'K} \delta_{JK'} \delta_{\alpha\beta'} \delta_{\alpha'\beta}, \end{aligned} \quad (\text{II. 12})$$

where $\langle \rangle$ denotes here and from now on an ensemble average.

Assumption (5) permits us to consider only random coupling models characterized by a Gaussian distribution. These are the two simplifying features which make our approach tractable.

The plausibility arguments provided for assumption (4) and (5) are by no means conclusive. We have recently undertaken a numerical investigation²⁶ which confirms these assumptions for all systems studied. Next, we introduce our mathematical technique using a simple soluble example.

III. ONE DISCRETE LEVEL INTERACTING WITH A SINGLE DENSE MANIFOLD-DIAGRAMMATIC APPROACH

The time evolution of an initially populated discrete level $|0\rangle$ interacting with a dense manifold $\{|1\alpha\rangle\}$ (Fig. 2) is easily soluble within the assumptions summarized by relation (II.10). On the timescale $t < \tau$ the population P_0 decays exponentially with the rate

$$\Gamma_{01} = 2\pi \langle V_{01}^2 \rangle \rho_1 \quad (III.1)$$

In what follows we describe the solution for this problem using the diagrammatic expansion technique with ensemble averaging, as an introduction to the more complicated cases discussed in the following sections.

The basic quantities that are calculated here are the averaged diadic and tetradic Green's functions which are related to the absorption line shape and to the time evolution (also to light scattering cross-sections), respectively. Relevant matrix elements of the tetradic Green's operator are related to those of the diadic Green's operator by

$$\begin{aligned} S_{bb,aa}(E) &= \frac{1}{2\pi i} \int_{-\infty}^{\infty} dU [G(U+i\eta)]_{ba} \{G^*[U-E+i(\eta'-\eta)]\}_{ba} \\ &= \frac{1}{2\pi i} \int_{-\infty}^{\infty} dU \left(\frac{1}{U-H+i\eta} \right)_{ba} \left(\frac{1}{U-E-H-i(\eta'-\eta)} \right)_{ab} \\ &\quad (\eta, \eta' > 0; \eta' > \eta) \quad (III.2) \end{aligned}$$

In terms of S , the probability that level $|b\rangle$ is occupied at time t given that level $|a\rangle$ was occupied at $t=0$ is

$$P_b(t) = -\frac{1}{2\pi i} \int_{-\infty}^{\infty} dE \exp(-iEt) S_{bb,aa}(E), \quad (III.3)$$

also, the absorption line shape $L(E)$ associated with a system whose initial state is $|a\rangle$ satisfies (for dipole induced transitions)

$$L(E) \propto -Im [\mu G(E) \mu]_{aa}, \quad (III.4)$$

where μ is the transition dipole operator.

Equations (III.3) and (III.4) represent observables expressed as linear functionals of the appropriate Green's functions. For systems corresponding to any of the RCM's introduced in Sec. II the evaluation of these expressions is grossly simplified by introducing ensemble averaged Green's functions. By assumption (4) of Sec. II this should not influence the final result. The Green's function elements appearing in Eqs. (III.3, 4) are thus replaced by the ensemble averages $\langle S_{bb,aa} \rangle$ and $\langle G_{aa} \rangle$, respectively. Furthermore, by assumption (5) of Sec. II we may limit ourselves to Gaussian randomness.

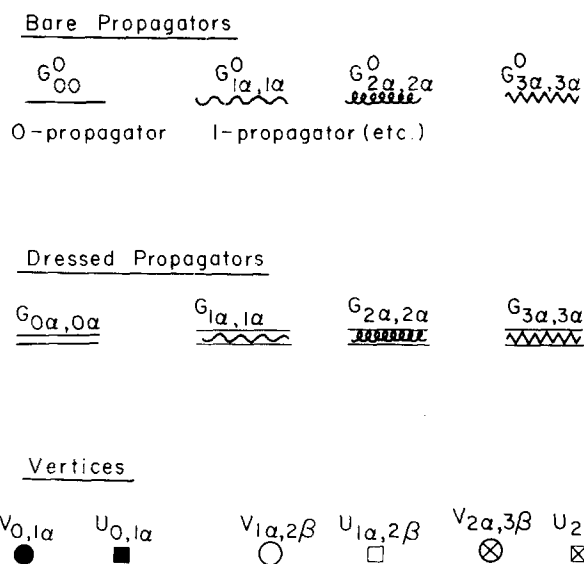


FIG. 3. Elementary diagrams used in the intercontinuum time evolution problem (Secs. III and IV). Shown are the notations for the 0-, 1-, 2-, and 3- bare propagators and for the corresponding dressed ones. Also shown are the different vertices which correspond to different r (random) and c - (constant) groups of matrix elements.

A. Evaluation of $\langle G_{00} \rangle$

We use the expansion

$$G_{00} = G_{00}^0 + G_{00}^0 \left(\sum_{\alpha} V_{0,1\alpha} G_{1\alpha,1\alpha}^0 V_{1\alpha,0} \right) G_{00}^0 + \dots, \quad (III.5)$$

where $G^0 = (E - H_0 + i\eta)^{-1}$, $\eta \rightarrow 0+$, and where $H_0 = H - V$. Consider first the symmetric RCM, with $V = v$, $\langle v \rangle = 0$. Introducing diagram elements appearing in Fig. 3, the expansion (III.5) becomes

$$\begin{aligned} \text{---} &= \text{---} + \text{---} \bullet \text{---} + \\ &\quad \text{---} \bullet \bullet \text{---} + \dots \quad (III.6) \end{aligned}$$

where (a) for a propagator line connecting two vertices a summation of the corresponding states is implied, and (b) each diagram is calculated as a product of its elements. Next we take an ensemble average of the expansion (III.6) term by term. Since we deal with Gaussian averages, an average of each diagram is performed by pairing the different vertices (coupling elements), taking the product of averages of pairs and summing over all the different pairing schemes. Diagrammatically an averaged pair will be denoted by the corresponding vertices connected by a dashed line. Thus for example

$$\begin{aligned} \langle \text{---} \bullet \text{---} \bullet \text{---} \bullet \text{---} \rangle &= \text{---} \bullet \text{---} \bullet \text{---} \bullet \text{---} \text{---} \\ &+ \text{---} \bullet \text{---} \bullet \text{---} \bullet \text{---} \text{---} \\ &+ \text{---} \bullet \text{---} \bullet \text{---} \bullet \text{---} \text{---} \quad (III.7) \end{aligned}$$

Note that Eq. (II.12) implies that when a dashed line connects vertices which belong to different 1-propagators, a summation over states is done for the product of

these propagators and not for each of them separately. It is easily realized that of the three diagrams appearing on the rhs of (III. 7) only the first is different from zero. The other two vanish because [using (II. 12)] they contain the factor

$$\sum_{\alpha} \frac{\langle v_{0,1\alpha}^2 \rangle}{(E - E_{1\alpha} + i\eta)^2} \approx \langle v_{0,1\alpha}^2 \rangle \rho_1 \int_{-\infty}^{\infty} dx \frac{1}{(E - x + i\eta)^2} = 0. \quad (\text{III. 8})$$

This is general, the rule being that only diagrams with pairing between vertices which belong to the same 1-propagator survive. The averaged expansion is thus

$$\begin{aligned} \langle \text{---} \rangle &= \text{---} + \text{---} \text{---} \text{---} + \text{---} \text{---} \text{---} \text{---} + \dots \\ &= \left[(\text{---})^{-1} - \text{---} \right]^{-1} \end{aligned} \quad (\text{III. 9})$$

or

$$\langle G_{00}(E) \rangle = (E - \bar{E}_0 + \frac{1}{2}i\Gamma_{01})^{-1}, \quad (\text{III. 10a})$$

where

$$\begin{aligned} \Gamma_{01} &= -2\text{Im} \sum_{\alpha} \frac{\langle v_{0,1\alpha}^2 \rangle}{E - E_{1\alpha} + i\eta} \\ &\approx 2\pi \langle v_{01}^2 \rangle \rho_1 \equiv \Gamma_{01}^{(r)}, \end{aligned} \quad (\text{III. 10b})$$

and where

$$\begin{aligned} \bar{E}_0 &= E_0 + D_{01}; \\ D_{01} &= PP \left(\sum_{\alpha} \frac{\langle v_{0,1\alpha}^2 \rangle}{E - E_{1\alpha}} \right) \equiv D_{01}^{(r)}. \end{aligned} \quad (\text{III. 10c})$$

Turning now to the more general asymmetric RCM, $V = u + v$ with $\langle V \rangle = u$, we note that (a) only diagrams with even numbers of random (r) vertices [and therefore also even number of constant (c) vertices] contribute to G and (b) the survival rule for averaged diagrams still holds: pairing may occur only between r -vertices which are nearest neighbors separated by 1-propagator. Then (III. 9) is replaced by

$$\begin{aligned} \langle \text{---} \rangle &= \text{---} + \text{---} \text{---} \text{---} + \text{---} \text{---} \text{---} \text{---} \\ &+ \text{---} \text{---} \text{---} \text{---} \text{---} + \text{---} \text{---} \text{---} \text{---} \text{---} \text{---} + \dots \\ &= \left[(\text{---})^{-1} - \text{---} \right]^{-1} \end{aligned} \quad (\text{III. 11})$$

so that (III. 10b, c) becomes

$$\begin{aligned} \Gamma_{01} &= 2\pi \langle u_{01}^2 + \langle v_{01}^2 \rangle \rangle \rho_1 \equiv \Gamma_{01}^{(c)} + \Gamma_{01}^{(r)} \\ D_{01} &= PP \left(\sum_{\alpha} \frac{u_{01}^2 + \langle v_{0,1\alpha}^2 \rangle}{E - E_{1\alpha}} \right) = D_{01}^{(c)} + D_{01}^{(r)}. \end{aligned} \quad (\text{III. 12})$$

B. Evaluation of $\langle G_{00,00} \rangle$

We first calculate the averaged product $\langle (u - H + i\eta)_{00}^{-1} \times (u - E - H - i\eta')_{00}^{-1} \rangle$. For this process we take the product of expansions of the two diadics. For the symmetric RCM the expansion (III. 6) yields

$$\begin{aligned} \langle \text{---} \rangle &= \text{---} + \text{---} \text{---} \text{---} + \text{---} \text{---} \text{---} \text{---} + \dots \\ &= \text{---} + \text{---} \text{---} \text{---} + \text{---} \text{---} \text{---} \text{---} + \dots \end{aligned} \quad (\text{III. 13})$$

Now each diagram is composed of two branches: the upper branch corresponds to $G(U + i\eta)$ while the lower one to $G^*(U - E - i\eta')$. Taking averages by pairing the r vertices as before we now encounter the possibility of pairing vertices from upper and lower branches. Thus

$$\begin{aligned} \langle \text{---} \rangle &= \text{---} + \text{---} \text{---} \text{---} + \text{---} \text{---} \text{---} \\ &+ \text{---} \text{---} \text{---} \text{---} \end{aligned} \quad (\text{III. 14})$$

A short calculation (Appendix A) shows that in the statistical limit ($\langle |v_{01}| \rangle \rho_1 \gg 1$) diagrams in which pairing occurs between r vertices from different branches are negligible relative to those in which pairing takes place within each branch separately. Neglecting the former we obtain for this model

$$\begin{aligned} \langle (U - H + i\eta)_{00}^{-1} (U - E - H - i\eta')_{00}^{-1} \rangle &= \langle (U - H + i\eta)_{00}^{-1} \rangle \langle (U - E - H - i\eta')_{00}^{-1} \rangle \\ &= (U - \bar{E}_0 + \frac{1}{2}i\Gamma_{01})^{-1} (U - E - \bar{E}_0 - \frac{1}{2}i\Gamma_{01})^{-1}, \end{aligned} \quad (\text{III. 15})$$

where in order to obtain the last equality Eq. (III. 10a) was used. Inserting this result into the averaged equivalent of Eq. (III. 2) leads to

$$\langle S_{00,00}(E) \rangle = (E + i\Gamma_{01})^{-1}, \quad (\text{III. 16})$$

where Γ_{01} is given by Eq. (III. 10b). In the presence of a constant coupling component the conditions which lead to Eq. (III. 14) still hold and we obtain again the result (III. 16) with Γ_{01} given by (III. 12).

These averaged diadic [Eq. (III. 10a)] and tetradic [Eq. (III. 16)] Green's function elements can be used to evaluate the line shape and time evolution using Eqs. (III. 3) and (III. 4). We note that the time evolution obtained from Eqs. (III. 3) and (III. 16)

$$P_0(t) = \exp(-\Gamma_{01}t) \quad (t > 0), \quad (\text{III. 17})$$

may be also obtained from the Fourier transform of the averaged diadic Green's function using the conventional expression²⁷ $|(2\pi)^{-1} \int_{-\infty}^{\infty} dE \exp(-iEt) \langle G_{00}(E) \rangle|^2$. This is not generally true: Only ensemble averages of observable quantities are meaningful and the averaged Green's function cannot be used for the evaluation of the time evolution which is quadratic in Green's function elements. For example, the averaged elements $\langle G_{1\alpha,0} \rangle$ vanish in the symmetric random case because in all orders such elements contain an odd number of random coupling elements. To calculate the time evolution of the $\{|1\alpha\rangle\}$ manifold the tetradic expansion has to be used.

In the following sections we apply the same method to calculations involving more complicated, physically relevant models.

IV. CONSECUTIVE TIME EVOLUTION

In this section we apply the technique described in the previous section to the more complicated problem of time evolution in systems involving several interacting manifolds.

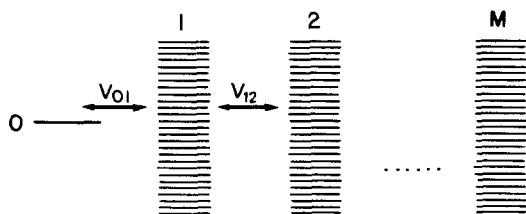


FIG. 4. Model used for the time evolution problem studied in Sec. IV.

Consider the model displayed in Fig. 4. The system is initially prepared in the state $|0\rangle$. We require the time evolution of the populations P_0, P_1, P_2, \dots of the state $|0\rangle$ and the manifolds 1, 2, etc. We assume that only "nearest neighbor" $0-1, 1-2, 2-3, \dots$ couplings are nonzero. The coupling elements satisfy the definitions of one of the models described in Sec. II.

The required populations satisfy

$$P_f(t) = -\frac{1}{2\pi i} \int_{-\infty}^{\infty} dE \exp\left(-i\frac{E}{\hbar}t\right) \bar{B}_f(E) \quad (\text{IV. 1a})$$

$$\bar{B}_f(E) = \frac{1}{2\pi i} \int_{-\infty}^{\infty} dU B_f(U, E) \quad (\text{IV. 1b})$$

where

$$B_0(U, E) = \langle [(U - H + i\eta)^{-1}]_{00} [(U - E - H - i\eta')^{-1}]_{00} \rangle \quad (\text{IV. 2a})$$

$$B_f(U, E) = \sum_{\alpha} \langle [(U - H + i\eta)^{-1}]_{f\alpha, 0} \times [(U - E - H - i\eta')^{-1}]_{\alpha, 0} \rangle. \quad (\text{IV. 2b})$$

Equation (IV. 2b) is equivalent to (III. 2) under our assumption that H is given as a real (therefore symmetric) infinite matrix in our representation.

A general term in the expansion of the tetradic Green's function is characterized by its order in the coupling V . The coupling elements belong to different groups defined by the manifolds they couple and by their random or constant nature. To each group we assign a given vertex form. Similarly, with each manifold we associate a different propagator form. These elementary diagrams are presented in Fig. 3. They are used to create the diagrams for the expansion of $\langle G_{ba}^+(U + i\eta) \times G_{ba}^+(U - E - i\eta) \rangle$ and to evaluate them according to the following rules:

(1) Create all the proper²⁸ combinations of free propagators and vertices using the given number of vertices of each type, arranging them in upper and lower branches (for terms arising from G_{ba} and G_{ba}^+ , respectively). These diagrams should start on their right with a propagators and on their left with b propagators (on both branches).

(2) From each diagram obtained in this way form the corresponding averaged diagrams by combining pairs of r vertices with dashed lines in all possible combinations. Any two vertices so connected are referred to as *connected vertices*.

(3) Propagator lines corresponding to a given manifold, which terminate on connected vertices are assigned the same index α corresponding to the individual

levels of this manifold.

Such propagator lines are referred to as *connected propagators*. A group of propagators, all corresponding to the same manifold, all connected within the group but without connections to any propagator outside the group is called *closely connected*. The smallest connected group consists of a single propagator. (For example the first of the three diagrams on the rhs of Eq. (III. 14) or Eq. (III. 7) consists of two singly connected 1-propagators. Each one of the other two diagrams contains one closely connected group of (two) 1-propagators.)

(4) Evaluate the diagram as the product of its elements, summing over all the free individual level indices α . Any pair of connected vertices contributes a $\langle V^2 \rangle$ factor.

Several observations may be made while evaluating such diagrams. We shall refer to these as the diagram selection rules:

(A) A closely connected group of propagators all lying on the same branch yields a vanishing factor (and therefore a vanishing diagram) unless the group consists of a single propagator. This results from the summation over the group level index which is of the form

$$\sum_{\alpha} [F(E_{\alpha})] \approx \rho \int dx [F(x)], \quad (\text{IV. 3})$$

where $F(x)$ is a product of propagators which, lying on the same branch, are analytic in either the upper or the lower complex x plane. Furthermore when more than one propagator is involved, $F(x) \rightarrow 0$ fast enough as $|x| \rightarrow \infty$ and contour integration shows that the integral in (IV. 3) vanishes.

(B) In any order of the expansion only diagrams with the largest number of summations (corresponding to the largest number of closely connected propagator groups) should be retained. The reason for this is that each α summation replaces an energy denominator by a density of states factor. The arguments presented in Appendix A then imply that each additional α summation makes the term larger by a factor $\epsilon \rho \gg 1$ (ϵ is defined in Sec. II).

(C) Any dashed line connecting an upper branch vertex to a lower branch one divides the diagram into two parts such that no other dotted lines connect the two parts. Again, breaking this rule results in diagrams which are smaller in order of $\epsilon \rho$ than equivalent diagrams which satisfy the rule.

The last rule implies the following result:

(D) Dashed lines connecting upper branch vertices to lower branch ones do not cross each other.

There is one exception to rule D, which involves connections between vertices of the type $v_{0,1}$. This point is discussed in Appendix B. To each diagram of the kind presented in Fig. 5(b) there is an equivalent counterpart of equal magnitude like in Fig. 5(a). Thus all diagrams may be selected according to rules C and D provided that those belonging to the exceptional group (the σ_0 diagrams discussed below) are multiplied by two.

Examples demonstrating the construction and evalua-

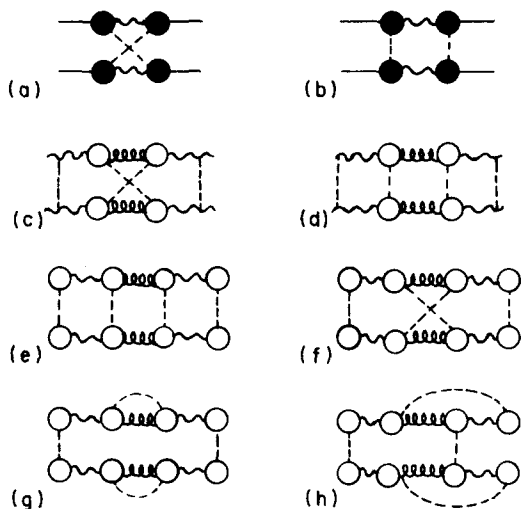


FIG. 5. Diagrams discussed in the text.

tion of the diagrams shown in Figs. 5 and 6 are presented in Appendices A and B. We now turn to the evaluation of the quantities B_0 and B_I [Eq. (IV.2)].

A. The symmetric RCM

We first limit ourselves to the symmetric RCM, taking $V = v$; $\langle v \rangle = 0$. Consider first the calculation of $B_0(u, E)$, Eq. (IV.2a). The first few terms in the expansion of this quantity are shown in Fig. 7. In general each diagram has segments which are separable into products of terms belonging to different branches and other segments which are nonseparable in this sense. The first step is the renormalization of the separable segments. We denote

$$\begin{aligned} \text{---} &= \text{---} + \text{---} \text{---} + \text{---} \text{---} \text{---} + \dots = \left[\left(\text{---} \right)^{-1} - \text{---} \right]^{-1} \\ &= \begin{cases} (U - \tilde{E}_0 + \frac{1}{2}i\Gamma_{01}^{(r)})^{-1} & \text{upper branch} \\ (U - E - \tilde{E}_0 - \frac{1}{2}i\Gamma_{01}^{(r)})^{-1} & \text{lower branch} \end{cases} \quad (\text{IV.4}) \end{aligned}$$

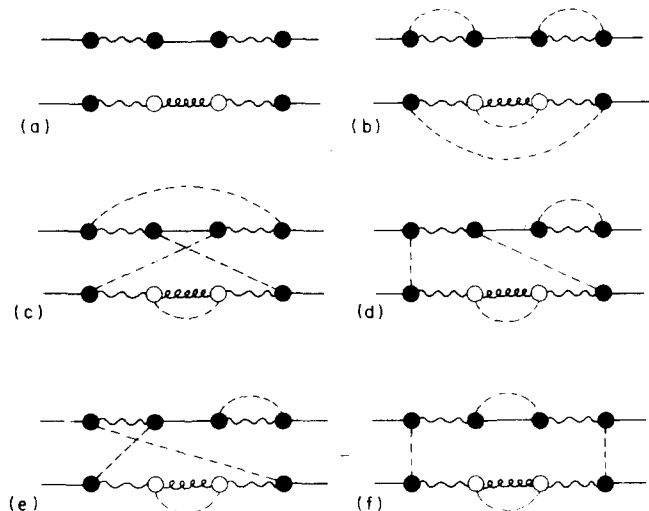
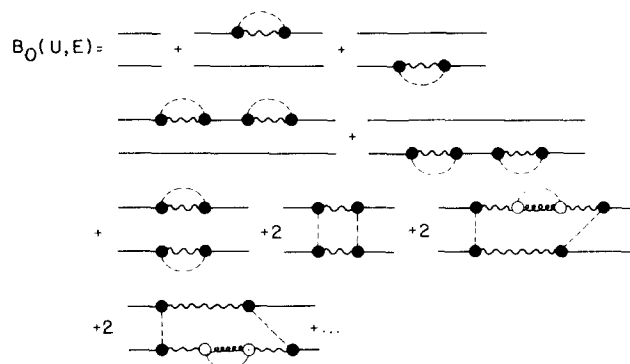


FIG. 6. Diagrams discussed in the text.

FIG. 7. Leading diagrams in the expansion of $B_0(U, E)$, Eq. (IV.2a).

$$\begin{aligned} \text{---} &= \text{---} + \text{---} \text{---} + \text{---} \text{---} \text{---} + \dots = \left[\left(\text{---} \right)^{-1} - \text{---} \right]^{-1} \\ &= \begin{cases} (U - \tilde{E}_{1\alpha} + \frac{1}{2}i\Gamma_{12}^{(r)})^{-1} & \text{upper branch} \\ (U - E - \tilde{E}_{1\alpha} - \frac{1}{2}i\Gamma_{12}^{(r)})^{-1} & \text{lower branch} \end{cases} \quad (\text{IV.5}) \end{aligned}$$

$$\begin{aligned} \text{---} &= \text{---} + \text{---} \text{---} + \text{---} \text{---} \text{---} + \dots = \left[\left(\text{---} \right)^{-1} - \text{---} - \text{---} \right]^{-1} \\ &= \begin{cases} [U - \tilde{E}_{2\alpha} + \frac{1}{2}i(\Gamma_{21}^{(r)} + \Gamma_{23}^{(r)})]^{-1} & \text{upper branch} \\ [U - E - \tilde{E}_{2\alpha} - \frac{1}{2}i(\Gamma_{21}^{(r)} + \Gamma_{23}^{(r)})]^{-1} & \text{lower branch} \end{cases} \quad (\text{IV.6}) \end{aligned}$$

In general a renormalized (averaged) diadic propagator has the form

$$\langle G_{I\alpha, I\alpha} \rangle = \begin{cases} [U - \tilde{E}_{I\alpha} + \frac{1}{2}i(\Gamma_{I, I-1}^{(r)} + \Gamma_{I, I+1}^{(r)})]^{-1} & \text{upper branch} \\ [U - E - \tilde{E}_{I\alpha} - \frac{1}{2}i(\Gamma_{I, I-1}^{(r)} + \Gamma_{I, I+1}^{(r)})]^{-1} & \text{lower branch} \end{cases} \quad (\text{IV.7})$$

where

$$\Gamma_{10}^{(r)} = \Gamma_{M, M+1}^{(r)} = 0; \quad \Gamma_{IJ}^{(r)} = 2\pi \langle v_{IJ}^2 \rangle \rho_J, \quad (\text{IV.8})$$

and where $\tilde{E}_{I\alpha}$ is the shifted energy

$$\tilde{E}_{I\alpha} = E_{I\alpha} + D_{I, I-1}^{(r)} + D_{I, I+1}^{(r)}$$

$$D_{10}^{(r)} = D_{M, M+1}^{(r)} = 0; \quad D_{IJ}^{(r)} = \text{Re} \left(\sum_{\alpha} \frac{\langle v_{IJ}^2 \rangle}{E - E_{J\alpha} + i\eta} \right). \quad (\text{IV.9})$$

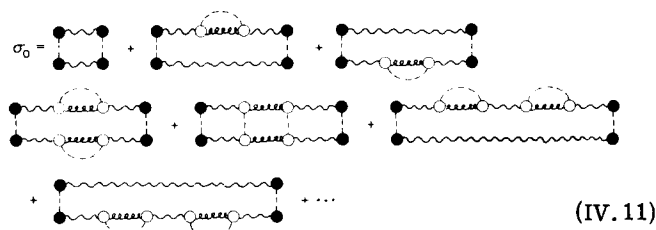
The index (r) denotes the random origin of these quantities.

In terms of the renormalized 0-propagators $B_0(U, E)$ takes the form

$$\begin{aligned} B_0(U, E) &= \text{---} + \text{---} \text{---} + \text{---} \text{---} \text{---} \\ &= \left[\left(\text{---} \right)^{-1} - 2\sigma_0 \right]^{-1} \end{aligned}$$

$$= [(U - \tilde{E}_0 + \frac{1}{2}i\Gamma_{01}^{(r)})(U - E - \tilde{E}_0 - \frac{1}{2}i\Gamma_{01}^{(r)} - 2\sigma_0)]^{-1} \quad (IV. 10)$$

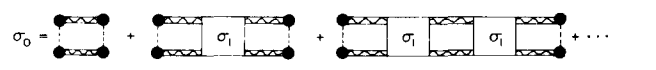
where σ_0 is the sum of nonseparable segments which start and end with vertical dashed lines connecting v_{01} vertices, having no other similar connections



$$\sigma_0 = \dots + \dots + \dots + \dots + \dots \quad (IV. 11)$$

The factor 2 in front of σ_0 in Eq. (IV. 10) is a symmetry factor discussed above and in Appendix B. The constructions of diagrams belonging to σ_0 is done following rules A-D above. In addition we note that v_{01} vertices in addition to the four located at the extreme ends should not appear in these diagrams. When such vertices appear inside σ_0 [e.g., Fig. 6(f)] we may always find a diagram of the same order in the coupling which is larger in order ($\epsilon\rho$) [compare Figs. 6(f) and 6(d)].

The calculation now boils down to the evaluation of σ_0 . It is easily realized that in terms of the renormalized 1-propagator, Eq. (IV. 5), σ_0 takes the form

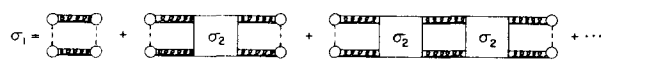


$$\sigma_0 = \dots + \dots + \dots + \dots \quad (IV. 12)$$

$$= \langle v_{01}^2 \rangle^2 \left[\left(\sum_{\alpha} \frac{1}{(U - \tilde{E}_{1\alpha} + \frac{1}{2}i\Gamma_{12}^{(r)})(U - E - \tilde{E}_{1\alpha} - \frac{1}{2}i\Gamma_{12}^{(r)})} \right) - \sigma_1 \right]^{-1}$$

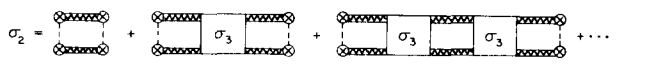
$$= 2\pi i \rho_1 \langle v_{01}^2 \rangle^2 [E + i\Gamma_{12}^{(r)} - 2\pi i \rho_1 \sigma_1]^{-1},$$

where σ_1 is the sum of non separable diagram segments which start and end with vertical dashed lines connecting v_{12} vertices, having no other similar connections. σ_1 is represented by the following partially resummed series



$$\sigma_1 = \dots + \dots + \dots + \dots \quad (IV. 13)$$

Similarly σ_2 is given by



$$\sigma_2 = \dots + \dots + \dots + \dots \quad (IV. 14)$$

and so on. Denoting

$$X_J = -2\pi i \rho_J \sigma_J \quad (IV. 15)$$

we obtain the following recursion relation

$$X_J = \frac{\Gamma_{J, J+1}^{(r)} \Gamma_{J+1, J}^{(r)}}{E + i(\Gamma_{J+1, J}^{(r)} + \Gamma_{J+1, J+2}^{(r)}) + X_{J+1}} \quad (IV. 16)$$

with

$$\Gamma_{10}^{(r)} = \Gamma_{M, M+1}^{(r)} = X_M = 0. \quad (IV. 17)$$

Equations (IV. 10), (IV. 16), and (IV. 15) now provide a complete solution for $B_0(U, E)$. It is seen that X in Eq.

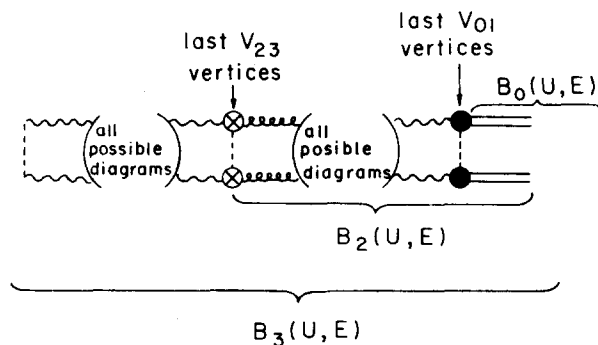


FIG. 8. A demonstration of the structure of diagrams corresponding to $B_J(U, E)$ terms [Eq. (IV. 2a)] for the symmetric RCM.

(IV. 16) is of order Γ and therefore σ is of order $\Gamma\rho^{-1}$. Comparing to the other term in Eq. (IV. 10) (which is of order Γ^2) we see that σ_0 may be disregarded in that equation. We get

$$B_0(U, E) = [(U - \tilde{E}_0 + \frac{1}{2}i\Gamma_{01}^{(r)})(U - E - \tilde{E}_0 - \frac{1}{2}i\Gamma_{01}^{(r)})]^{-1} \quad (IV. 18)$$

Inserting into Eq. (IV. 1) leads to

$$P_0(t) = \exp(-\Gamma_{01}^{(r)} t). \quad (IV. 19)$$

Thus in the symmetric RCM the time evolution of the initial state $|0\rangle$ is not affected by the presence of manifolds other than that directly coupled to it. We shall see that this result does not hold in the asymmetric case.

Next consider the calculation of $B_J(U, E)$, $J=1, 2, \dots, M$. This can be easily achieved by referring to Fig. 8. The diagram representing $B_J(U, E)$ starts with 0-propagators on the right and with J -propagators on the left. Identifying the first position, going from left to right, where a vertical dashed line connects two $v_{J, J-1}$ vertices, we see that the diagram segment on its left is essentially σ_{J-1} while on its right we have $B_{J-1}(U, E)$. We obtain

$$B_J(U, E) = \langle v_{J, J-1}^2 \rangle^{-1} \sigma_{J-1} B_{J-1}(U, E) \quad (IV. 20)$$

Also using (IV. 1b)

$$\bar{B}_J(E) = \langle v_{J, J-1}^2 \rangle^{-1} \sigma_{J-1} \bar{B}_{J-1}(E). \quad (IV. 21)$$

Together with [from Eqs. (IV. 1b) and (IV. 18)]

$$\bar{B}_0(E) = \frac{1}{E + i\Gamma_{01}^{(r)}}, \quad (IV. 22)$$

and with Eqs. (IV. 15, 16), this provides the complete solution for the Fourier Laplace transform $\bar{B}_J(E)$ of $P_J(t)$.

It may be now easily seen that Eqs. (IV. 1a), (IV. 15, 16), and (IV. 21) imply that the populations $P_J(t)$ satisfy the set of kinetic equations

$$\begin{aligned} \dot{P}_0(t) &= -k_{01}^{(r)} P_0(t) \\ \dot{P}_J(t) &= -(k_{J, J+1}^{(r)} + k_{J, J-1}^{(r)}) P_J(t) + k_{J-1, J}^{(r)} P_{J-1}(t) \\ &\quad + k_{J+1, J}^{(r)} P_{J+1}(t) \quad J=1, 2, \dots, M-1 \end{aligned} \quad (IV. 23)$$

$$P_M(t) = -k_{M, M-1}^{(r)} P_M(t) + k_{M-1, M}^{(r)} P_{M-1}(t),$$

where

$$k_{JJ'}^{(r)} = \Gamma_{JJ'}^{(r)} / \hbar. \quad (IV. 24)$$

To see this we note that

$$\dot{P}_J(t) = -(2\pi i)^{-1} \int_{-\infty}^{\infty} dE \left(-i \frac{E}{\hbar} \right) \exp \left(-i \frac{E}{\hbar} t \right) \bar{B}_J(E) \quad (IV. 25)$$

and that Eqs. (IV. 15), (IV. 16), and (IV. 21) may be rearranged to give

$$-iE\bar{B}_J = -(\Gamma_{J,J-1}^{(r)} + \Gamma_{J,J+1}^{(r)})\bar{B}_J + \Gamma_{J-1,J}^{(r)}\bar{B}_{J-1} + \Gamma_{J+1,J}^{(r)}\bar{B}_{J+1}. \quad (IV. 26)$$

Equations (IV. 1a), (IV. 25), and (IV. 26) lead directly to result (IV. 23). Thus, in the symmetric RCM the populations of the different manifolds satisfy a regular Pauli master equation. This result does not rely on a weak coupling assumption or a repeated random phase approximation as do conventional theories.¹⁹

B. The asymmetric RCM

We now examine the modifications which enter into the result (IV. 23) when the randomness is taken to be asymmetric: $V = u + v$, $\langle v \rangle = 0$, $\langle V \rangle = u$. We assume that both constant and random coupling components satisfy the statistical limit criterion $\langle |v| \rangle \rho$, $|u| \rho \gg 1$. Also we first limit ourselves in the following discussion to a system having one discrete state $|0\rangle$ and two manifolds $\{|1\alpha\rangle\}$ and $\{|2\alpha\rangle\}$ ($M=2$ in Fig. 4), and discuss the general case later.

We start again with the calculation of $B_0(U, E)$ and, as before, the first step is the normalization of the 0-propagator. To this end we note that any diagram in the expansion of $\langle G_{00} \rangle$ must be separable into products of terms involving either random coupling or constant coupling but not both. This results from vanishing of mixed terms, e.g.,

$$\text{Diagram 1} = \text{Diagram 2} = \text{Diagram 3} = \text{Diagram 4} \quad (IV. 27)$$

according to rule A for diagram selection. The renormalized 0-propagator therefore takes the form

$$\text{Diagram 5} = \left[\text{Diagram 6}^{-1} - \text{Diagram 7} - \text{Diagram 8} \right]^{-1} \quad (IV. 28)$$

where

$$\text{Diagram 8} = \text{Diagram 9} + \text{Diagram 10} + \text{Diagram 11} + \dots \quad (IV. 29)$$

is the sum of single branch diagrams which (1) contain only constant coupling vertices, (2) terminate on either side with u_{01} vertices, and (3) do not contain any additional u_{01} vertex. This series may be resummed to yield

$$\text{Diagram 12} = \frac{\text{Diagram 13}}{1 + N_{12}} \quad (IV. 30)$$

where

$$N_{IJ} = - \sum_{\alpha_1} \sum_{\alpha_2} \frac{u_{IJ}^2}{(U - E_{I\alpha_1} + i\eta)(U - E_{J\alpha_2} + i\eta)} \quad (IV. 31)$$

and where the numerator on the rhs of (IV. 30) is the diagrammatic representation of

$$\sum_{\alpha} \frac{u_{01}^2}{U - E_{1\alpha} + i\eta} \equiv D_{01}^{(c)} - \frac{1}{2} i \Gamma_{01}^{(c)} \quad (IV. 32)$$

with

$$\Gamma_{01}^{(c)} = 2\pi u_{01}^2 \rho_1; \quad D_{01}^{(c)} = PP \left(\sum_{\alpha} \frac{u_{01}^2}{U - E_{1\alpha} + i\eta} \right). \quad (IV. 33)$$

Note that Eqs. (IV. 31-33) are written for upper branch diagrams. The corresponding lower branch equations are obtained by replacing U by $U - E$ and taking complex conjugate. Equation (IV. 28) may be now written in the explicit form

$$\langle G_{00} \rangle = \begin{cases} [U - \bar{E}_0 + \frac{1}{2} i (\Gamma_{01}^{(r)} + \bar{\Gamma}_0^{(c)})]^{-1} & \text{for upper branch} \\ [U - E - \bar{E}_0 - \frac{1}{2} i (\Gamma_{01}^{(r)} + \bar{\Gamma}_0^{(c)})]^{-1} & \text{for lower branch} \end{cases} \quad (IV. 34)$$

where

$$\bar{E}_0 = E_0 + D_{01}^{(r)} + \frac{D_{01}^{(c)}(1 + \text{Re}N_{12}) - \frac{1}{2} \Gamma_{01}^{(c)} \text{Im}N_{12}}{(1 + \text{Re}N_{12})^2 + (\text{Im}N_{12})^2}, \quad (IV. 35)$$

$$\bar{\Gamma}_0^{(c)} = \frac{\Gamma_{01}^{(c)}(1 + \text{Re}N_{12}) + 2D_{01}^{(c)} \text{Im}N_{12}}{(1 + \text{Re}N_{12})^2 + (\text{Im}N_{12})^2}, \quad (IV. 36)$$

and where $\Gamma_{01}^{(r)}$ and $D_{01}^{(r)}$ are defined in Eqs. (IV. 8, 9). We note in passing that in the many continua case these results are still valid, only N_{12} is replaced by \bar{N}_{12} defined by

$$\bar{N}_{I-1, I} = N_{I-1, I} / (1 + \bar{N}_{I, I+1}); \quad N_{M, M+1} = 0. \quad (IV. 37)$$

In the case where the principal part of the summations in (IV. 31) may be disregarded we obtain the more familiar forms

$$N_{IJ} = \pi^2 u_{IJ}^2 \rho_I \rho_J \quad (IV. 38)$$

and

$$\bar{\Gamma}_0^{(c)} = \Gamma_{01}^{(c)} / (1 + \bar{N}_{12}). \quad (IV. 39)$$

Next consider nonseparable segments [segments which cannot be represented as products of factors originating each from a different branch of the diagram contributing to $B_0(U, E)$]. In the symmetric RCM case such segments were resummed to yield the renormalized tetradic vertex σ_0 , which in turn was shown to be negligible relative to the inverse renormalized tetradic 0-propagator. In the present case it may again be shown (Appendix C) that nonseparable segments may be disregarded. This leads to the result [analogous to Eq. (IV. 18)]

$$B_0(U, E) = \{ [U - \bar{E}_0 + \frac{1}{2} i (\Gamma_{01}^{(r)} + \bar{\Gamma}_0^{(c)})] \times [U - E - \bar{E}_0 - \frac{1}{2} i (\Gamma_{01}^{(r)} + \bar{\Gamma}_0^{(c)})] \}^{-1}, \quad (IV. 40)$$

which leads to [using (IV. 1)]

$$P_0(t) = \exp[-(\Gamma_{01}^{(r)} + \bar{\Gamma}_0^{(c)})t]. \quad (IV. 41)$$

Turning now to the calculation of $B_I(U, E)$, $I=1, 2$, we note first the general structure of the corresponding diagrams. The diagrams belonging to $B_1(U, E)$ and $B_2(U, E)$ are of the forms displayed in Fig. 9. The main common feature here is that each diagram contains

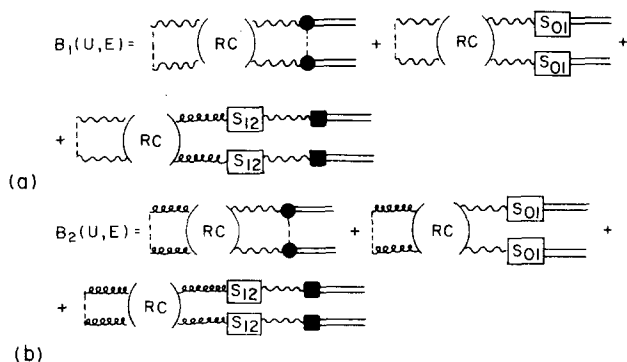


FIG. 9. Diagrams appearing in the expansion of $B_J(U, E)$ terms ($J = 1, 2$) in the asymmetric RCM. The segments denoted by RC contain only random vertices. The segment S_{12} is defined in Fig. 10.

three regions: Going from right to left these are (1) a $B_0(U, E)$ factor which is obtained from separable segments terminating on their left in black (v_{01} or u_{01}) vertices, (2) a constant coupling (CC) region which may be resummed to yield the normalized forms S_{01} and S_{12} (defined in Appendix C and in Fig. 10), and finally (3) a random coupling (RC) region which starts and ends with vertical dashed lines connecting r vertices on the two branches. The renormalized c vertices [Eqs. (C1–C4)] have small magnitudes and therefore CC insertions inside the RC region are disregarded in the spirit of Appendix C. The CC region preceding (going from right to left) the RC region is needed in order to keep track of the possibility that random coupling is absent altogether. The reader should convince himself that diagrams which do not conform with the forms presented in Fig. 9 may indeed be disregarded according to the diagram selection rules.

The diagrams appearing in Fig. 9 are evaluated by using

$$\text{RC} = \langle v_{01}^2 \rangle^{-2} \sigma_0 \quad (IV. 42)$$

$$\begin{aligned} \text{RC} \text{---} \text{RC} &= \text{RC} \text{---} \text{RC} = \text{RC} \text{---} \text{RC} = \\ &= \langle v_{12}^2 \rangle^{-1} \sigma_1 \langle v_{01}^2 \rangle^{-2} \sigma_0 \end{aligned} \quad (IV. 43)$$

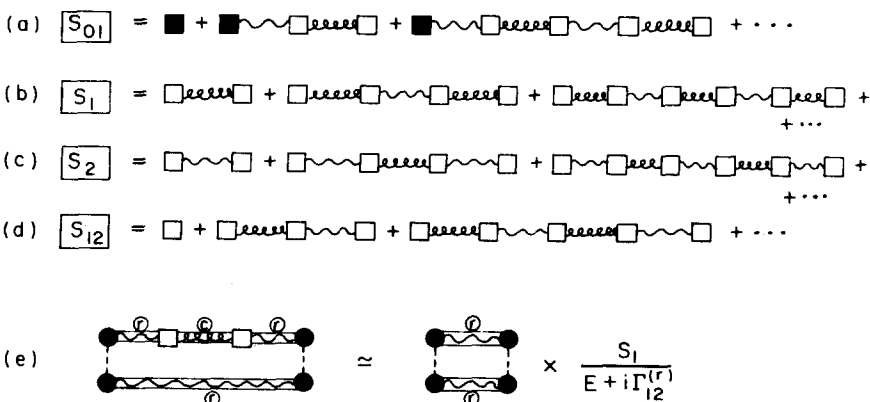


FIG. 10. Diagrams referred to in the discussion of time evolution in the asymmetric RCM. Renormalized propagators denoted by Ir and c correspond to renormalization with only the random or only the constant coupling component, respectively.

$$\text{RC} = \frac{\text{RC}}{\text{RC}} + \frac{\text{RC}}{\text{RC}} \text{---} \text{RC} = \langle v_{12}^2 \rangle^{-2} \sigma_1 (1 + \sigma_1 \langle v_{01}^2 \rangle^{-2} \sigma_0)$$

with σ_0 and σ_1 given by Eqs. (IV. 15, 16) namely

$$\sigma_0 = i \langle v_{01}^2 \rangle \Gamma_{01}^{(r)} [E + i \Gamma_{12}^{(r)} + \Gamma_{12}^{(r)} \Gamma_{21}^{(r)} (E + i \Gamma_{21}^{(r)})^{-1}]^{-1} \quad (IV. 45a)$$

$$\sigma_1 = i \langle v_{12}^2 \rangle \Gamma_{12}^{(r)} (E + i \Gamma_{21}^{(r)})^{-1} \quad (IV. 45b)$$

Assuming for simplicity that N_{12} is real and given by (IV. 38) we obtain

$$\begin{aligned} B_1(U, E) &= (1 + \langle v_{01}^2 \rangle^{-4} S_{01}^2 + \langle v_{12}^2 \rangle^{-4} \pi^2 \rho_1^2 u_{01}^2 \langle v_{01}^2 \rangle^{-4} S_{12}^2) \\ &\quad \times \langle v_{01}^2 \rangle^{-4} \sigma_0 B_0(U, E) \end{aligned} \quad (IV. 46)$$

$$\begin{aligned} B_2(U, E) &= \langle v_{12}^2 \rangle^{-4} \sigma_1 [\langle v_{12}^2 \rangle^{-4} \pi^2 \rho_1^2 S_{12}^2 u_{01}^2 B_0(U, E) \\ &\quad + B_1(U, E)] \end{aligned} \quad (IV. 47)$$

Inserting these results into Eq. (IV. 1b) leads to the corresponding expressions for $\bar{B}_1(E)$ and $\bar{B}_2(E)$, the only change being the conversion of the $B_0(U, E)$ term in Eqs. (IV. 46, 47) into $\bar{B}_0(E) = [E + i(\Gamma_{01}^{(r)} + \bar{\Gamma}_0^{(c)})]^{-1}$. It may be easily shown that these expressions for $\bar{B}_I(E)$ are identical to the Fourier Laplace transforms of $P_I(t)$ ($I = 0, 1, 2$) which satisfies the rate equations

$$\dot{P}_0(t) = -[\Gamma_{01}^{(r)} + \Gamma_{01}^{(c)} / (1 + N_{12})] P_0(t) \quad (IV. 48)$$

$$\begin{aligned} \dot{P}_1(t) &= [\Gamma_0^{(r)} + (1 + N_{12})^{-2} \Gamma_{01}^{(c)}] P_0(t) \\ &\quad - \Gamma_{12}^{(r)} P_1(t) + \Gamma_{21}^{(r)} P_2(t) \end{aligned} \quad (IV. 49)$$

$$\begin{aligned} \dot{P}_2(t) &= [N_{12} / (1 + N_{12})^2] \Gamma_{01}^{(c)} P_0(t) \\ &\quad + \Gamma_{12}^{(r)} P_1(t) - \Gamma_{21}^{(r)} P_2(t) \end{aligned} \quad (IV. 50)$$

Generalization of this calculation to the several manifold case ($M > 2$ in Fig. 4) is not completely straightforward, the reason being that the renormalized c vertices [Eqs. (C1–4)] are not always small. For example in the three manifolds case ($M = 3$ in Fig. 4) the factor N_{12} is replaced by $\bar{N}_{12} = N_{12} / (1 + N_{23})$ [cf. Eq. (IV. 37)] which is of order unity for $N \gg 1$. There is however another important situation where the present calculation is valid: In the many manifolds case (large M in Fig. 4) continued fractions of the kind defined in Eq. (IV. 37) are large for $N \gg 1$. For example for $M \rightarrow \infty$ and taking all N to be equal, we obtain

$$\bar{N} = \frac{N}{1 + \frac{N}{1 + \frac{N}{1 + \dots}}} \approx N^{1/2} \quad (\text{for } N \gg 1) \quad (IV. 51)$$

The renormalized c -vertices [Eqs. (C1-4)] are therefore again small and the diagram selection procedure may be carried out as for the $M=2$ case. In particular the pattern observed in the diagrams contributing to B_1 and B_2 (Fig. 9) is maintained and the results for $B_I(U, E)$ ($I=0, 1, 2$) is obtained as a direct extension of the procedure described above. This leads to results for $\bar{B}_I(E)$ [Eqs. (IV. 1b)] which are identical to the Fourier Laplace transforms of the quantities $P_I(t)$ satisfying the kinetic equations

$$\dot{P}(t) = \mathbf{k}P(t), \quad (IV. 52)$$

where $P = (P_0 P_1 \dots P_M)$ and where the rate matrix \mathbf{k} may be represented as a sum of the two matrices

$$\mathbf{k} = \mathbf{k}^{(c)} + \mathbf{k}^{(r)}. \quad (IV. 53)$$

$\mathbf{k}^{(r)}$ is determined by the random coupling component. Its nonzero elements are

$$\begin{aligned} k_{J,J}^{(r)} &= -(\Gamma_{J,J-1}^{(r)} + \Gamma_{J,J+1}^{(r)})/\hbar \\ k_{J,J\pm 1}^{(r)} &= \Gamma_{J\pm 1,J}^{(r)}/\hbar \end{aligned} \quad (IV. 54)$$

with $\Gamma^{(r)}$ defined by Eq. (IV. 8). $\mathbf{k}^{(c)}$ includes the rates induced by the constant coupling component and its nonzero elements are

$$\begin{aligned} k_{00}^{(c)} &= -C_1 \Gamma_{01}^{(c)}/\hbar; \quad k_{10}^{(c)} = C_1^2 \Gamma_{01}^{(c)}/\hbar \\ k_{J,0}^{(c)} &= C_J \left[\prod_{j=1}^{J-1} (1 - C_j) \right] C_1 \Gamma_{01}^{(c)}/\hbar, \end{aligned} \quad (IV. 55)$$

where $\Gamma_{01}^{(c)}$ is given by Eq. (IV. 33) and where the coefficients C_J are defined from

$$\begin{aligned} C_M &= 1 \\ C_J &= (1 + N_{J,J+1} C_{J+1})^{-1} \quad J=1, 2, \dots, M-1. \end{aligned} \quad (IV. 56)$$

In writing these results we have assumed that the numbers $N_{J,J'}$ are real and thus given by Eq. (IV. 38).

The following points should be noted concerning this result:

(a) The random coupling and the constant coupling components induce two separate rate processes. The constant coupling component induces a coherent, simultaneous transition from the initial level to each of the manifolds. The random component induces a consecutive process with rates given by the golden rule expression.

(b) In the cases considered here ($M=2$ and M large) the contribution of the constant coupling component is much smaller than that of the random one and may be disregarded as long as $|u|$ is not much larger than $\langle |v| \rangle$. For intermediate M we expect deviations from this conclusion.

(c) The results (IV. 52-56) satisfy the limiting cases: For $u \rightarrow 0$ we obtain the symmetric RCM result, Eq. (IV. 23). For $v \rightarrow 0$ we get the CCM result known from earlier work.^{20,30}

(d) Consider the two manifolds case with $u_{01} = v_{12} = 0$; that is a random coupling between the state $|0\rangle$ and the manifold $\{|1\alpha\rangle\}$ and a constant (or rather smooth) coupling between the two manifolds. Expressions (IV. 48,

50) predict that on the time scale for which these results hold [given by Eq. (II. 10)] no transition occurs between the two manifolds. We have shown before¹⁰ that this is a characteristic feature of the separable RCM for which a constant coupling constitutes a special case. A diagrammatic approach to the separable RCM is presented in Appendix D.

(e) In the calculations presented in this paper, we are considering cases where the random coupling component is not correlated, e. g., for the separable RCM

$$\langle v_{I\alpha} v_{I'\alpha'} \rangle = \langle v_I^2 \rangle \delta_{II'} \delta_{\alpha\alpha'}. \quad (IV. 57)$$

We have treated before¹⁰ the separable RCM in the presence of correlations, where

$$\langle v_{I\alpha} v_{I'\alpha'} \rangle = \langle v_I^2 \rangle f(E_{I\alpha} - E_{I'\alpha'}), \quad (IV. 58)$$

taking a Lorentzian model for f

$$f(E_{I\alpha} - E_{I'\alpha'}) = \bar{\epsilon}^2 / [(E_{I\alpha} - E_{I'\alpha'})^2 + \bar{\epsilon}^2]. \quad (IV. 59)$$

For the ensemble average approach to be valid the "correlation length" $\bar{\epsilon}$ must be small, of order ϵ [Eq. (II. 10)] or less. It is interesting to note that the 1-2 transition rate, predicted to vanish in the zero-correlation separable RCM (Appendix D) is of order $\bar{\epsilon}$ in the model represented by Eqs. (IV. 58, 59).

(f) The results obtained in this section were tested by numerical simulations for two and three manifold models²⁶ and were found to hold well. Interestingly, the analytical and simulation results remain in good agreement with each other also for times much larger than the theoretical validity range $\tau \sim \rho$. This seems to be a general feature of RCM's, where the random nature of the coupling leads to a substantial increase in the recurrence times.

V. ERASURE OF INTERFERENCE FEATURES IN ABSORPTION LINE SHAPES

In this section we present the diagrammatic expansion approach to the calculation of absorption line shapes. The simple single resonance case has been treated in Sec. III: The ensemble averaged line shape is obtained using [cf. Eq. (III. 4)]

$$L(E) \propto -\text{Im}(\mu \langle G(E) \rangle \mu)_{aa}, \quad (V. 1)$$

where a is the initial (absorbing) state. For a simple isolated resonance (Fig. 2), Eq. (V. 1) leads to

$$L(E) \propto -|\mu_{01}|^2 \text{Im} \langle G_{00}(E) \rangle \quad (V. 2)$$

and [using Eq. (III. 10a)]

$$L(E) \propto |\mu_{01}|^2 / [(E - \bar{E}_0)^2 + (\frac{1}{2}\Gamma_{01})^2]. \quad (V. 3)$$

Γ_{01} is [cf. Eq. (III. 12)] the sum of contributions from the constant and the random coupling components.

Typical interference features arise when the width of resonances exceeds their spacing or when the underlying continuum $\{|1\alpha\rangle\}$ (Fig. 2) is also optically active. Such cases are usually treated under the assumption that the coupling between the discrete levels and between the quasicontinuous manifold is smooth, essentially a constant coupling situation. The role of randomness in such

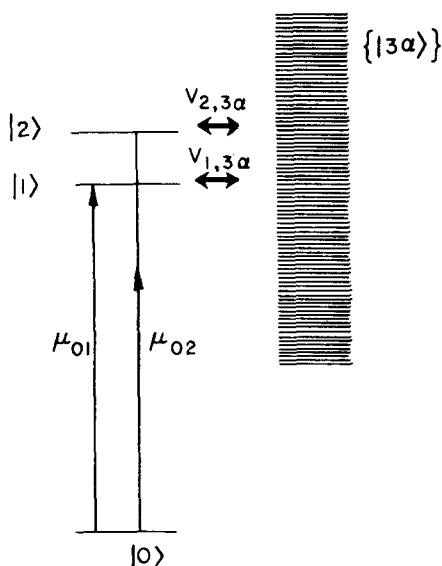


FIG. 11. Excitation involving two resonances.

models has been recently discussed by Druger.⁸ Here we apply the ensemble average idea together with the diagrammatic expansion approach to these problems.

The applicability of the ensemble average procedure for time evolution problems rests on the existence of a large number of states within the uncertainty width of the levels. This sets an upper time limit τ for the validity of these results [Eq. (II.10)]. A line shape experiment is characterized by an energy resolution width $\delta\omega$, and ensemble averaging is meaningful only if $\delta\omega \gg \rho^{-1}$, i.e., there are enough levels within the width $\delta\omega$ so that the distribution of random couplings is reliably sampled at any excitation energy. Denoting by ΔE the width of the spectral features of interest the validity criterion for our approach is therefore

$$\rho^{-1} \ll \delta\omega \ll \Delta E, \tag{V.5}$$

which replaces for line shape problems the criterion (II.10). Under the same conditions we expect that Gaussian random models are sufficiently general as discussed in Sec. II.

A. Two overlapping resonances

Consider the model displayed in Fig. 11 where the ground state $|0\rangle$ is radiatively coupled³¹ (with matrix elements μ_{01} and μ_{02}) to the discrete states $|1\rangle$ and $|2\rangle$ which are in turn coupled to the radiatively inert manifold $\{|3\alpha\rangle\}$. We assume

$$\begin{aligned} V_{1,3\alpha} &= v_{1,3\alpha} + u_{1,3} ; & V_{2,3\alpha} &= v_{2,3\alpha} + u_{2,3} \\ \langle v_{1,3\alpha} \rangle &= \langle v_{2,3\alpha} \rangle = 0 \\ \langle v_{1,3\alpha} v_{1,3\alpha'} \rangle &= \langle v_{1,3}^2 \rangle \delta_{\alpha\alpha'} \\ \langle v_{2,3\alpha} v_{2,3\alpha'} \rangle &= \langle v_{2,3}^2 \rangle \delta_{\alpha\alpha'} \\ \langle v_{1,3\alpha} v_{2,3\alpha'} \rangle &= 0. \end{aligned} \tag{V.5}$$

The absorption line shape takes the form

$$\begin{aligned} L(E) \propto & -Im(|\mu_{01}|^2 \langle G_{11}(E) \rangle + |\mu_{02}|^2 \langle G_{22}(E) \rangle \\ & + \mu_{01}\mu_{20} \langle G_{21}(E) \rangle + \mu_{02}\mu_{10} \langle G_{12}(E) \rangle), \end{aligned} \tag{V.6}$$

so that we need to calculate four elements of the averaged Green's operator $G = (E - H + i\eta)^{-1}$, $\eta \rightarrow 0^+$. We demonstrate our approach by considering the simpler case where only state $|1\rangle$ is optically active, $\mu_{02} = 0$. Then

$$L(E) \propto -|\mu_{01}|^2 Im \langle G_{11}(E) \rangle. \tag{V.7}$$

The elementary diagrams for these problems are shown in Fig. 12(a). The diagram selection rule A (Sec. IV) imply that dashed lines may connect only nearest neighbor vertices which are connected by a 3-propagator. G_{11} is given by $G_{11} = (E - E_1 - \sigma_1)^{-1}$ where the self-energy σ_1 is the sum of all diagrams bounded on both sides by u_{13} or v_{13} vertices, which do not contain any 1-propagator. There are three contributions to σ_1 , shown on Fig. 12(b). Disregarding level shifts we obtain

$$\begin{aligned} \langle G_{11}(E) \rangle = & \left[E - E_1 + \frac{1}{2}i(\Gamma_{13}^{(r)} + \Gamma_{13}^{(c)}) \right. \\ & \left. + \frac{\frac{1}{4}\Gamma_{13}^{(c)}\Gamma_{13}^{(c)}}{E - E_2 + \frac{1}{2}i(\Gamma_{23}^{(r)} + \Gamma_{23}^{(c)})} \right]^{-1}, \end{aligned} \tag{V.8}$$

which should be inserted into (V.7). In the random case where $\Gamma_{13}^{(c)} \cdot \Gamma_{23}^{(c)} = 0$ this leads to a simple Lorentzian: the optically active level $|1\rangle$ does not "feel" the presence of level $|2\rangle$. Note that for this to be true it is sufficient that one of the two levels is coupled randomly to the quasicontinuum. If $\Gamma_{13}^{(c)} \cdot \Gamma_{23}^{(c)} \neq 0$ (i.e., both levels have a smoothly varying coupling component with the quasicontinuum) interference affects sets in. In the absence of a random coupling component the result (V.8) reduces to that obtained in previous works.³²

When $\mu_{02} \neq 0$ the same method may be used to obtain the other needed elements of $\langle G \rangle$. In particular we note that since G_{12} and G_{21} are odd in either v_{13} or v_{23} their

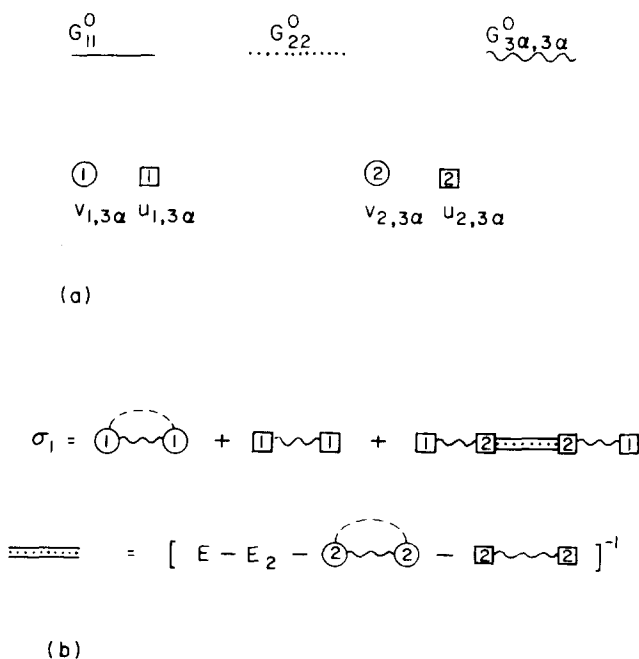


FIG. 12. Diagrams used in the discussion of line shapes involving two overlapping resonances. (a) Elementary diagrams (b) Renormalized propagator and self energy.

average must vanish in the symmetric RCM. In this case all interference effects are erased and Eq. (V.6) results in a linear combination of two simple Lorentzians associated with the two resonances.

B. The Fano lineshape³³

Next we consider the model shown in Fig. 13: The ground state $|0\rangle$ is radiatively coupled to a discrete state $|1\rangle$ and to a quasicontinuum $\{|2\alpha\rangle\}$ with dipole elements μ_{01} and $\mu_{0,2\alpha}$.³¹ Also the state $|1\rangle$ and the manifold 2 are coupled with elements $V_{1,2\alpha}$. $\mu_{0,2\alpha}$ and $V_{1,2\alpha}$ are taken to be random

$$\begin{aligned} V_{1,2\alpha} &= v_{1,2\alpha} + u_{1,2} \\ \mu_{0,2\alpha} &= (\delta\mu)_{0,2\alpha} + \langle\mu_{0,2}\rangle, \end{aligned} \tag{V.9}$$

where the random components v and $\delta\mu$ satisfy equations similar to (V.5).

Elementary diagrams for this problem are defined in Fig. 14(a). The different contributions to the element $(\mu G\mu)_{00}$ whose imaginary part is proportional to the absorption lineshape are shown in Fig. 14(b). The terms A–D (evaluated with level shifts disregarded)

$$(A) = |\mu_{0,1}|^2 / [E - E_1 + \frac{1}{2}i(\Gamma_{1,2}^{(r)} + \Gamma_{1,2}^{(c)})] \tag{V.10}$$

$$(B) = -i\pi\langle\mu_{0,2}\rangle^2\rho_2 = -\frac{1}{2}i\Gamma_{02}^{(c)} \tag{V.11}$$

$$(C) = -\frac{1}{4}\Gamma_{0,2}^{(c)}\Gamma_{1,2}^{(c)} / [E - E_1 + \frac{1}{2}i(\Gamma_{1,2}^{(r)} + \Gamma_{1,2}^{(c)})] \tag{V.12}$$

$$(D) = -2\pi i\rho_2\langle\mu_{0,2}\rangle u_{1,2} \mu_{0,1} / [E - E_1 + \frac{1}{2}i(\Gamma_{1,2}^{(r)} + \Gamma_{1,2}^{(c)})] \tag{V.13}$$

are standard and appear also in the original Fano theory (the only difference lies in the additional random coupling width of the Lorentzian associated with state $|1\rangle$). The last term in Fig. 14(b)

$$(E) = -\frac{1}{2}i\Gamma_{0,2}^{(r)} = -i\pi\langle\delta\mu_{0,2\alpha}^2\rangle\rho_2 \tag{V.14}$$

represents an additional background absorption resulting from the random 0–2 coupling. The line shape resulting from these contributions takes the form

$$\begin{aligned} L(E) &\propto \frac{1}{2}(\Gamma_{0,2}^{(r)} + \Gamma_{0,2}^{(c)}) + \frac{1}{4}\Gamma_{0,2}^{(c)}\Gamma_{1,2}^{(c)} \\ &\times \frac{\frac{1}{2}(q^2 - 1)(\Gamma_{1,2}^{(r)} + \Gamma_{1,2}^{(c)}) + 2q(E - E_1)}{(E - E_1)^2 + \frac{1}{4}(\Gamma_{1,2}^{(r)} + \Gamma_{1,2}^{(c)})^2}, \end{aligned} \tag{V.15}$$

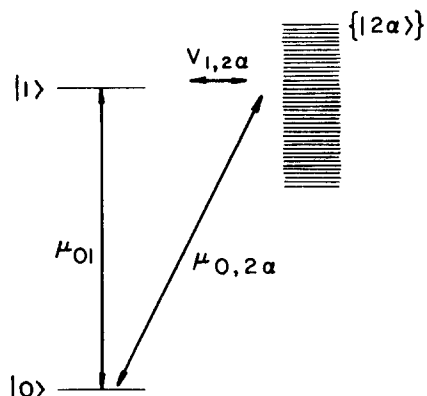


FIG. 13. Excitation involving a single resonance interacting with an absorbing continuum (the Fano problem).

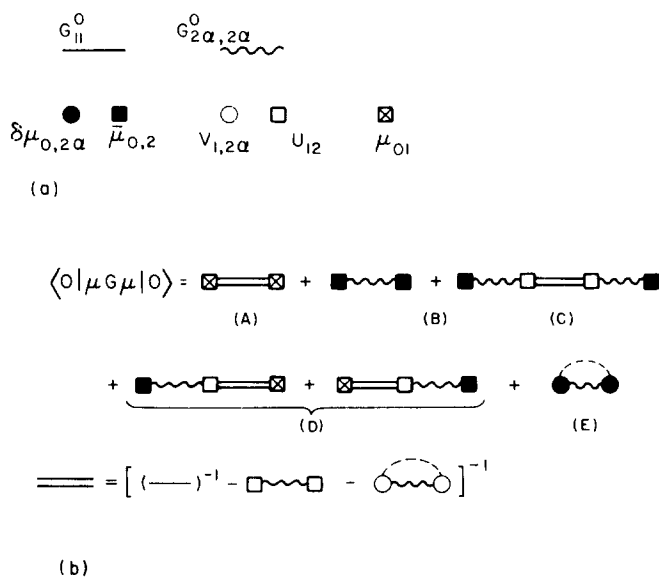


FIG. 14. Diagrams involved in the discussion of the Fano problem with random coupling. (a) Elementary diagrams (b) Diagrams contributing to the line shape.

where

$$q = \mu_{0,1} / \pi\rho_2\langle\mu_{0,2}\rangle u_{1,2}, \tag{V.16}$$

when $v_{1,2} = \delta\mu_{0,2} = 0$ for all α , the coupling is smooth and Eq. (V.15) reduces to the familiar Fano result

$$\begin{aligned} L(E) &\propto \frac{1}{2}\Gamma_{0,2}^{(c)}(E - E_1 + \frac{1}{2}\Gamma_{1,2}^{(c)})^2 / \\ &[(E - E_1)^2 + (\frac{1}{2}\Gamma_{1,2}^{(c)})^2]. \end{aligned} \tag{V.17}$$

On the other hand, in the symmetric RCM $\langle\mu_{0,2}\rangle = u_{1,2} = 0$ and we obtain

$$\begin{aligned} L(E) &\propto \frac{1}{2}\Gamma_{1,2}^{(r)}|\mu_{01}|^2 / [(E - E_1)^2 + (\frac{1}{2}\Gamma_{1,2}^{(r)})^2] \\ &+ \pi\langle\delta\mu_{0,2}^2\rangle\rho_2 \end{aligned} \tag{V.18}$$

showing that the line shape in this case reduces to a linear combination of a Lorentzian (arising from the discrete level $|1\rangle$) and the continuous background absorption, without any interference between them. Note that such a form arises also when either the ground state $|0\rangle$ or the excited state $|1\rangle$ couple randomly with the quasicontinuum. In practice, of course, the presence or absence of random coupling will characterize both states simultaneously.

Equation (V.15) represents a continuous transition from the Fano result (V.17) to the Lorentzian on background form (V.18) as the random nature of the coupling increases. Introducing the quantities

$$\begin{aligned} \lambda &= \langle\mu_{0,2}\rangle u_{1,2} / \sqrt{(\langle\mu_{0,2}\rangle^2 + \langle\delta\mu_{0,2\alpha}^2\rangle)(u_{1,2}^2 + \langle v_{1,2\alpha}^2\rangle)} \\ &= \begin{cases} 1 & \text{(purely constant coupling)} \\ 0 & \text{(purely random coupling)} \end{cases} \end{aligned} \tag{V.19}$$

$$Q = \lambda q = \mu_{0,1} / \pi\rho_2 \sqrt{(\langle\mu_{0,2}\rangle^2 + \langle\delta\mu_{0,2\alpha}^2\rangle)(u_{1,2}^2 + \langle v_{1,2\alpha}^2\rangle)} \tag{V.20}$$

$$\epsilon_2 = E - E_1 / \pi\rho_2(u_{1,2}^2 + \langle v_{1,2\alpha}^2\rangle) \tag{V.21}$$

$$L_0 = \pi\rho_2(\langle\mu_{0,2}\rangle^2 + \langle\delta\mu_{0,2\alpha}^2\rangle) \tag{V.22}$$

we obtain

$$L(E) = L_0(Q^2 + 2Q\lambda\epsilon_2 + \epsilon_2^2 + 1 - \lambda^2)/(\epsilon_2^2 + 1). \quad (\text{V. 23})$$

This result is identical to that obtained earlier by Druger⁸ (for the case where all transition dipoles are parallel) who used an approach based on Fano's configuration interaction method.³³ We note that the solution (V. 23) was obtained in an approximation which takes the radiative interaction up to second order. The same approximation was used by Fano and, following him, by Druger.

In the CCM, a solution to the Fano problem has been obtained³⁴ which is not limited in this way. Our approach enables us to avoid this approximation also in the random coupling case. In this case we encounter coupling between the quasicontinuum $\{|2\alpha\rangle\}$ and the continuum of one-photon states $\{|0\beta\rangle\}$ seating on the molecular ground state $|0\rangle$. Denoting by ρ_0 the density of levels in this radiative continuum and defining the inter-continuum coupling parameters

$$N^{(c)} = \pi^2 \langle \mu_{0,2} \rangle^2 \rho_0 \rho_2 \quad (\text{V. 24})$$

$$N^{(r)} = \pi^2 \langle \delta \mu_{0,2} \rangle^2 \rho_0 \rho_2 \quad (\text{V. 25})$$

we obtain by extending the diagrammatic expansion technique

$$L(E) = \frac{\frac{1}{2} \Gamma_{0,2}^{(c)}}{1 + N^{(c)} + N^{(r)}} \left[\left(1 + \frac{N^{(r)}}{N^{(c)}} \right) + \frac{1 + N^{(c)}}{1 + N^{(c)} + N^{(r)}} \frac{\Gamma_{1,2}^{(c)} q^2 + 2q\epsilon - 1}{\epsilon^2 + 1} \right], \quad (\text{V. 26})$$

where

$$\Gamma_1 = \Gamma_{1,0}^{(c)} + \Gamma_{1,2}^{(c)} + \Gamma_{1,2}^{(r)} \quad (\text{V. 27a})$$

$$\Gamma_{1,0}^{(c)} = 2\pi \rho_0 \mu_{1,0}^2 / (1 + N^{(c)} + N^{(r)}) \quad (\text{V. 27b})$$

$$\Gamma_{1,2}^{(c)} = 2\pi \rho^2 \mu_{1,2}^2 / (1 + N^{(c)}) \quad (\text{V. 27c})$$

$$\Gamma_{1,2}^{(r)} = 2\pi \rho_2 \langle v_{1,2}^2 \rangle \quad (\text{V. 27d})$$

$$\epsilon = (E - E_1 + D) / \Gamma_1 \quad (\text{V. 28})$$

and where

$$D = 2\pi^2 \rho_0 \rho_2 \mu_{12} \langle \mu_{02} \rangle \mu_{10} / (1 + N^{(c)} + N^{(r)}). \quad (\text{V. 29})$$

In the CCM limit where $v = \delta\mu = 0$, also $\Gamma_{12}^{(r)} = N^{(r)} = 0$ and Eq. (V. 26) reduces to the result obtained earlier³⁴

$$L(E) \propto \frac{\frac{1}{2} \Gamma_{0,2}^{(c)}}{1 + N^{(c)}} \left(1 + \frac{\Gamma_{1,2}^{(c)} q^2 + 2q\epsilon - 1}{\Gamma_1 \epsilon^2 + 1} \right). \quad (\text{V. 30})$$

In the purely random case, $\langle \mu_{0,2} \rangle = \mu_{1,2} = 0$, we have $N^{(c)} = \Gamma_{0,2}^{(c)} = \Gamma_{1,2}^{(c)} = 0$ and then we obtain

$$L(E) \propto \frac{\frac{1}{2} \Gamma_{0,2}^{(r)}}{1 + N^{(r)}} + \left(\frac{\mu_{0,1}}{1 + N^{(r)}} \right)^2 \frac{1}{\frac{1}{2} \Gamma_1} \cdot \frac{1}{\epsilon^2 + 1} \quad (\text{V. 31})$$

showing again that the line shape reduces in this limit to a superposition of a Lorentzian and a continuous background absorption. Equations (V. 26), (V. 30), and (V. 31) represent the corrected forms of Eqs. (V. 15), (V. 17), and (V. 18), respectively, where all orders in the radiative interactions are included.

The results (V. 15) [or (V. 26)] should be used as a basis for discussing Fano interference features in ab-

sorption line shapes of large molecules. Recently Sage and Jortner³⁵ have applied the result (V. 15) for their discussion of overtone absorption spectra in Benzene³⁶ and Naphthalene.³⁷ The appearance of an almost perfect Lorentzian feature superimposed on a continuous absorption provides a strong indication to the presence of random radiative coupling in these molecules.

VI. CONCLUSION

In this paper we have presented a method which allows us to obtain explicit solutions for the spectral properties and the dynamic behavior of systems which are characterized by essentially random coupling between manifolds of quantum levels. Such models are essential in understanding the behavior of large molecules in highly excited states. The main tools that we used: the ensemble average assumption and the diagrammatic expansion and averaging technique, lead to a substantial simplification of the problems studied, and enabled us to obtain explicit solutions for observable quantities in both the time and the energy domains. The method is useful for various molecular dynamics problems. Application to the theory of multiphoton excitation of large molecules is described in a subsequent paper. A random coupling model for the theory of light scattering off large molecule is currently under study.

ACKNOWLEDGMENTS

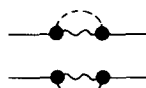
We are grateful to Professor J. Jortner and Mr. I. Schek for many helpful discussions.

APPENDIX A

Here we discuss the relative order of different diagrams in the statistical limit $\sqrt{\langle V^2 \rangle} \rho \gg 1$. We note that as the characteristic experimental timescale τ is often of order $\hbar \langle \langle V^2 \rangle \rangle^{-1}$, assumption (II. 10) is consistent with the statistical limit which qualitatively implies that width of levels greatly exceeds their spacing.

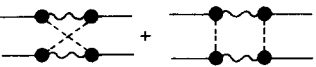
By assumption (II. 10) there exist in this limit an energy scale ϵ satisfying $\hbar/\tau \gg \epsilon \gg \rho^{-1}$. We discuss the magnitudes of diagrams in terms of the parameter $\epsilon \rho \gg 1$. To this end we associate with each level a width ϵ implying a finite lifetime \hbar/ϵ . This should not affect the physical results on a time scale $\tau \ll \hbar/\epsilon$. Furthermore ϵ is negligible relative to the real physical widths, e.g., $\epsilon \ll 2\pi \langle V^2 \rangle \rho$.

Consider now the diagrams appearing on the rhs of Eq. (III. 14). The first, with unconnected upper and lower branches yields



$$= [G_{00}^0(U+i\epsilon)G_{00}^0(U-E-i\epsilon)]^2 \times \sum_{\alpha} \frac{\langle v_{01}^2 \rangle}{U-E_{1\alpha}+i\epsilon} \sum_{\alpha} \frac{\langle v_{01}^2 \rangle}{U-E-E_{1\alpha}-i\epsilon} \approx \frac{\pi^2 \langle v_{01}^2 \rangle^2 \rho_1^2}{(U-E_0+i\epsilon)^2 (U-E-E_0-i\epsilon)^2}. \quad (\text{A1})$$

The other two diagrams are equal and give



$$= [G_{00}^0(U+i\epsilon)G_{00}^0(U-E-i\epsilon)]^2$$

$$\times \sum_{\alpha} \frac{\langle v_{0,1}^2 \rangle^2}{(U-E_{1\alpha}+i\epsilon)(U-E-E_{1\alpha}-i\epsilon)}$$

$$\simeq \frac{2\pi i \langle v_{0,1}^2 \rangle^2 \rho_1}{(U-E_0+i\epsilon)^2 (U-E-E_0-i\epsilon)^2 (E+2i\epsilon)}. \quad (\text{A2})$$

The ratio between the contributions in (A1) and (A2) is essentially $|\rho_1(E+2i\epsilon)| > \rho_1\epsilon \gg 1$. Thus connected branch diagrams may be disregarded. More rigorously, consider the contributions of these terms to the time evolution $P_0(t)$. The term in (A1) yields [using Eqs. (III. 2, 3)] and disregarding factors which appear both in (A1) and in (A2) $\rho_1(t/\hbar)^2 \exp[-2(\epsilon/\hbar)t]$, while the term in (A2) results in $(t/\hbar)^3 \exp[-2(\epsilon/\hbar)t]$. On the relevant time scale $t \ll \hbar\rho$ the latter may be disregarded.

APPENDIX B

Consider the diagram in Fig. 6(a) which represents the term (belonging to $S_{00,00}$)

$$\sum_{\alpha_1} \sum_{\alpha_2} \sum_{\alpha_3} \sum_{\alpha_4} \sum_{\alpha_5} v_{0,1\alpha_1}^2 v_{0,1\alpha_2}^2 v_{0,1\alpha_3} v_{0,1\alpha_4} v_{1\alpha_3,2\alpha_5}$$

$$\times v_{2\alpha_5,1\alpha_4} (U-E_{1\alpha_1}+i\eta)^{-1} (U-E_{1\alpha_2}+i\eta)^{-1} (U-E_0+i\eta)^{-1}$$

$$\times (U-E-E_{1\alpha_3}-i\eta')^{-1} (U-E-E_{1\alpha_4}-i\eta')^{-1}$$

$$\times (U-E-E_{2\alpha_5}-i\eta')^{-1} (U-E-E_0-i\eta')^{-1}.$$

Taking an ensemble average we obtain fifteen diagrams, five of which are presented in Figs. 6(b-f). Figure 6(b) vanishes, because it contains a closely connected group with more than one propagator lying purely on the lower branch. Comparing 6(c) and 6(d) we see that they differ in the fact that 6(c) contains one closely connected group of 1-propagators, while 6(d) contain two such groups. Figure 6(c) therefore represents a term which is smaller by a factor of $\epsilon\rho$ (ϵ defined in Sec. II) than the term represented by 6(d), and may be disregarded. Figure 6(e) is equivalent to 6(d). Figure 6(f) is of the same order as 6(c) and may also be disregarded.

Note that Fig. 6(c) involves connections which are forbidden by rules C and D of Sec. IV. To see this more clearly consider the diagrams in Fig. 5. Figures 5(e) and 5(g) each contain three closely connected propagator groups: 5(e) contains two groups of 1-propagators and one group of 2-propagators; 5(g) contains one group of 1-propagators and 2 groups of 2-propagators while Figs. 5(f) and 5(h) contain only two closely connected propagator groups (one of 1- and the other of 2-propagators). These diagrams, which are forbidden by rules C and D of Sec. IV may thus be disregarded.

Note that while the Fig. 5(f) is negligible relative to 5(e), this is not the case with Fig. 6(e) relative to 6(d). To understand the difference compare the diagrams in Figs. 5(a-d). Figures 5(a) and 5(b) are obviously of the same magnitude. In Figs. 5(c) and 5(d) however, we have a different situation because whenever they appear the configuration is such that the 1-propagators on the

two ends belong to a connected group [compare Figs. 5(e-h)]. This is schematically represented by the extra dashed lines appearing in Figs. 5(c) and 5(d). Figure 5(c) having only two closely connected propagator groups is therefore negligible relative to Fig. 5(d).

APPENDIX C

Here we estimate the relative contribution of non-separable diagram segments appearing in the expansion of $B_0(U, E)$ in the asymmetric RCM. For this purpose it will be useful to define the renormalized quantities represented diagrammatically in Figs. 10(a-d).

$$S_{01} = u_{01}/(1+N_{12}) \quad (\text{C1})$$

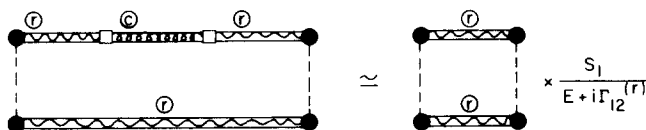
$$S_1 = (D_{12}^{(c)} - \frac{1}{2}i\Gamma_{12}^{(c)})/(1+N_{12}) \quad (\text{C2})$$

$$S_2 = (D_{21}^{(c)} - \frac{1}{2}i\Gamma_{21}^{(c)})/(1+N_{12}) \quad (\text{C3})$$

$$S_{12} = u_{12}/(1+N_{12}). \quad (\text{C4})$$

Note that the results in Eqs. (C2) and (C3) are written for upper branch quantities. The corresponding lower branch quantities are obtained by taking complex conjugates.

Nonseparable segments in $B_0(U, E)$ may be obtained either by connecting a group of r vertices [to yield renormalized tetrads vertex σ_0 , Eq. (IV.11)] or by connecting a group containing both r and c vertices. By examining diagrams of the later type one sees that they may be represented as essentially a product of a diagram from the σ_0 expansion and the factor $S/(E+i\Gamma^{(r)})$. For example



$$\approx \times \frac{S_1}{E+i\Gamma_{12}^{(r)}}$$

Assuming that $\Gamma^{(c)}$ and $\Gamma^{(r)}$ are of the same order, the factor $|S/(E+i\Gamma)|$ is of order N_{12}^{-1} which by our own assumption ($u\rho \gg 1$) is very small. We conclude that non-separable segments in the expansion of $B_0(U, E)$ may be disregarded.

APPENDIX D: THE SEPARABLE RCM

Here we present the outline of the calculation of the time evolution in a model consisting of one (initially populated) discrete level and two quasicontinua ($M=2$ in Fig. 4) where the intercontinuum coupling elements $v_{1\alpha,2\beta}$ are assumed to satisfy

$$v_{1\alpha,2\beta} = v_{1\alpha}v_{2\beta}, \quad (\text{D1})$$

where

$$\langle v_{1\alpha} \rangle = \langle v_{2\beta} \rangle = \langle v_{1\alpha}v_{2\beta} \rangle = 0. \quad (\text{D2})$$

The elementary diagrams are shown in Fig. 15(a). The separability of $v_{1\alpha,2\beta}$ is taken into account by expressing it as a double vertex. Averaging is carried out by pairing the corresponding half-vertices [see Figs. 15(b, d)]. It is found by inspecting these diagrams that the diagram selection rules formulated in Sec. IV also hold for the separable case.

The calculation of $B_0(U, E)$ [Eq. (IV.2)] involves as in

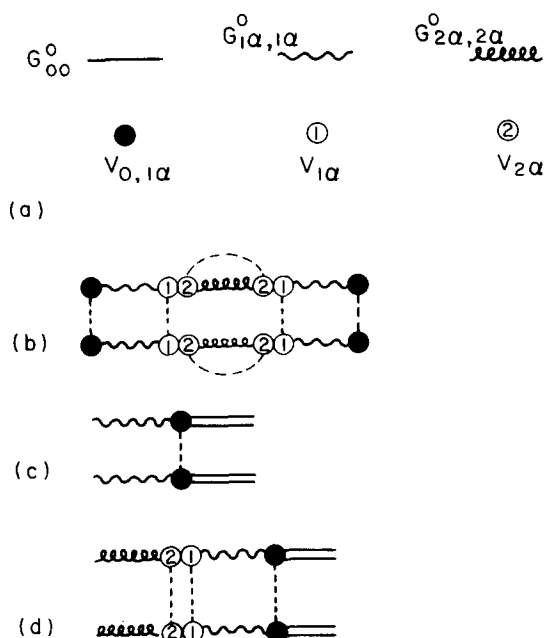


FIG. 15. Diagrams involved in the calculation of time evolution associated with the separable RCM. (a) Elementary diagrams (b)–(d) Diagrams used in the discussion of Appendix D.

Sec. IV the renormalized 0-propagator defined as in Eq. (IV.4), and the renormalized tetradic vertex σ_0 . In the nonseparable RCM σ_0 is given by (IV.11). In the separable case the diagrams are modified. For example the 4th and 5th diagrams on the rhs of (IV.11) are replaced by the diagram shown in Fig. 15(b). It may be easily confirmed that pairing schemes other than that represented by Fig. 15(b) result in contributions of lower order in $\epsilon\rho$ (ϵ defined in Sec. II). Summing diagrams of this kind it is realized that (as in the nonseparable case) σ_0 is negligible relative to the product of unconnected branch contribution, and we obtain

$$B_0(U, E) = [(U - \tilde{E}_0 + \frac{1}{2}i\Gamma_{01})(U - E - \tilde{E}_0 - \frac{1}{2}i\Gamma_{01})]^{-1}, \quad (\text{D4})$$

where $\Gamma_{01} = 2\pi\langle v_{01}^2 \rangle \rho_1$. The calculation of $B_1(U, E)$ leads to a sum whose leading term is shown in Fig. 15(c).

Inspection of this sum reveals that this leading term is larger (in order $\epsilon\rho$) than the sum over the rest of the terms. Keeping this term only we obtain

$$B_1(U, E) = \{i\Gamma_{01}/[E + i(\eta + \eta')]\} B_0(U, E). \quad (\text{D5})$$

Finally, evaluating $B_2(U, E)$ we encounter a series with the leading term given by Fig. 15(d). Summation of this series yields

$$B_2(U, E) = \{2iN/(1+N)^2\pi\rho_1[E + i(\eta + \eta')]\} B_1(U, E), \quad (\text{D6})$$

where

$$N \equiv \pi^2 \langle v_1^2 \rangle \langle v_2^2 \rangle \rho_1 \rho_2. \quad (\text{D7})$$

Under our assumptions the result (D7) is negligible and $B_2 \approx 0$. Using also Eqs. (D4) and (D5) together with Eq. (IV.1) we obtain

$$\begin{aligned} P_0(t) &= \exp(-\Gamma_{01}t) \\ P_1(t) &= 1 - \exp(-\Gamma_{01}t) \\ P_2(t) &= 0. \end{aligned} \quad (\text{D8})$$

This result indicates that on a time scale which satisfies (II.10) no transition occurs between the manifolds 1 and 2, in agreement with Ref. 10.

- ¹(a) S. A. Rice, in *Excited States*, edited by E. C. Lim (Academic, New York, 1975); (b) S. A. Rice: "Internal Energy Transfer in Isolated Molecules: Ergodic and Nonergodic Behavior," to be published. (c) R. A. Marcus, *Ber. Bunsenges Phys. Chem.* **81**, 190 (1970).
- ²W. M. Gelbart, S. A. Rice, and K. F. Freed, *J. Chem. Phys.* **57**, 4699 (1972).
- ³J. M. Delory and C. Tric, *Chem. Phys.* **3**, 54 (1974).
- ⁴W. M. Gelbart, D. F. Heller, and M. L. Elert, *Chem. Phys.* **7**, 116 (1975).
- ⁵K. G. Kay, *J. Chem. Phys.* **61**, 5205 (1974).
- ⁶E. J. Heller and S. A. Rice, *J. Chem. Phys.* **61**, 936 (1974).
- ⁷M. Muthukumar and S. A. Rice, *J. Chem. Phys.* **69**, 1619 (1978).
- ⁸S. D. Druger, *J. Chem. Phys.* **67**, 3238; 3249 (1977).
- ⁹J. Jortner, *Adv. Laser Spectrosc.* **113**, 88 (1977).
- ¹⁰B. Carmeli and A. Nitzan, *Chem. Phys. Lett.* **58**, 310 (1978).
- ¹¹B. Carmeli and A. Nitzan, *Chem. Phys. Lett.* (in press).
- ¹²I. Schek and J. Jortner, *J. Chem. Phys.* **70**, 3016 (1979).
- ¹³A. Nitzan and J. Jortner, *Chem. Phys. Lett.* (in press).
- ¹⁴E. P. Wigner, *Ann. Math. Lpz.* **62**, 548 (1955); **67**, 325 (1958).
- ¹⁵R. J. Elliott, J. A. Krumhansl and Leath, *Rev. Mod. Phys.* **46**, 465 (1974).
- ¹⁶B. Carmeli and A. Nitzan, *J. Chem. Phys.* **72**, 2010 (1980); following paper.
- ¹⁷B. Carmeli and A. Nitzan, to be published.
- ¹⁸For a discussion of this point see Ref. 10.
- ¹⁹(a) W. Pauli, *Festschrift zur 60. Geburtstag A. Sommerfelds* (Hirzel, Leipzig, 1928). (b) L. Van Hove, *Physica* **21**, 517 (1955). (c) R. Zwanzig, *Lecture Notes in Theoretical Physics III* (Interscience, New York, 1961), p. 106.
- ²⁰S. Mukamel and J. Jortner, *Mol. Phys.* **27**, 1543 (1974).
- ²¹S. Mukamel and J. Jortner, *J. Chem. Phys.* **60**, 4760 (1974).
- ²²J. A. Beswick and J. Jortner, *J. Chem. Phys.* **68**, 2277 (1978).
- ²³O. Atabek, J. A. Beswick, R. Lefebvre, S. Mukamel, and J. Jortner, *Mol. Phys.* **31**, 1 (1976).
- ²⁴M. Quack, *J. Chem. Phys.* **69**, 1282 (1978).
- ²⁵S. Mukamel, *Phys. Rev. Lett.* **42**, 168 (1979); *J. Chem. Phys.* **70**, 5834 (1979).
- ²⁶B. Carmeli, I. Schek, A. Nitzan, and J. Jortner, *J. Chem. Phys.* **72**, 1928 (1980).
- ²⁷M. L. Goldberger and R. M. Watson, *Collision Theory* (Wiley, New York, 1969).
- ²⁸Note that the type of vertex determines the type of the propagators attached to it.
- ²⁹This holds rigorously provided that the integration limits can be extended to $\pm\infty$.
- ³⁰A. Nitzan, J. Jortner, and B. J. Berne, *Mol. Phys.* **28**, 281 (1977).
- ³¹To avoid unnecessary complications we assume that all radiative coupling elements are parallel.
- ³²A. Nitzan and J. Jortner, *J. Chem. Phys.* **57**, 3870 (1972).
- ³³(a) U. Fano, *Phys. Rev.* **124**, 1866 (1961); (b) U. Fano and J. W. Cooper, *Phys. Rev.* **137**, A1364 (1965); *Rev. Mod. Phys.* **40**, 441 (1965).
- ³⁴(a) A. Nitzan, *Mol. Phys.* **27**, 65 (1974). (b) S. Mukamel and J. Jortner, *J. Chem. Phys.* **61**, 227 (1974).
- ³⁵M. L. Sage and J. Jortner, *Chem. Phys. Lett.* (in press).
- ³⁶R. G. Bray and M. J. Berry, *J. Chem. Phys.* (to be published).
- ³⁷J. W. Perry and A. H. Zewail, *J. Chem. Phys.* **70**, 582 (1979).